國立交通大學
光電工程研究所
碩士學位論文

使用波長掃描式脈衝光源之新型群速度色散量測技術

New group velocity dispersion measurement technique by using periodic wavelength-scanning pulse light source

研究生：劉秀鳳

指導教授：賴暎杰

中華民國九十八年六月

使用波長掃描式脈衝光源之新型群速度色散量測技術

New group velocity dispersion measurement technique by using periodic wavelength-scanning pulse light source

研 究 生：劉秀鳳　　Student：Shiou-Fong Liu

指導教授：賴暎杰 老師　　Advisor：Yin-Chieh Lai

國 立 交 通 大 學

光 電 工 程 研 究 所

碩 士 論 文

A Thesis

Submitted to Institute of Electronics College of Engineering

National Chiao Tung University

in partial Fulfillment of the Requirements

for the Degree of

Master

In Electro-Optical Engineering

June 2009

Hsinchu, Taiwan, Republic of China

中華民國九十八年六月

國 立 交 通 大 學

論文口試委員會審定書

本 校 光 電 工 程 研 究 所 碩 士 班 劉秀鳳 君

所提論文 利用波長掃描脈衝光源之群速度量測方法

合 於 碩 士 資 格 標 準 、業 經 本 委 員 會 評 審 認 可 。

口試委員：祁甦 許根玉

（祁甦 教授） （許根玉 教授）

彭朋群

（彭朋群 助理教授）

指導教授：郭哲

所　　長：張振加 教授

系 主 任：黃中玄 教授

中 華 民 國 98 年 6 月 24 日

摘　要

論文名稱：使用波長掃描式脈衝光源之新型群速度色散量測技術
校所別：國立交通大學光電工程研究所　　頁數：1 頁
畢業時間：九十七學年度第二學期　　學位：碩士
研究生：劉秀鳳　　指導教授：賴暎杰 老師

群速度色散係數在高速通訊、非線性光學及超快光學等很多科學與應用研究上扮演著重要的角色，本論文提出一種新型色散量測的方法及架構，只需使用射頻頻譜分析儀來觀測週期性光頻率掃描的時域脈衝頻譜即可求得群速度色散值。論文中所使用的光源為非同步鎖模光固子光纖雷射，此乃實驗室先前發展的架構，並有著令人感興趣的特性，例如：脈衝的時間位置與中心頻率具慢速週期性變化等。此外，我們也提出以頻率調制器與振幅調制器所架設的光源來產生中心頻率週期性變化的脈衝光源的新想法。將此類具慢速週期變化特性的光源之輸出光脈衝序列通過待測光纖，藉由直接分析通過待測光纖前後的光脈衝序列之射頻頻譜圖來獲得脈衝時間位置慢速週期性變化的大小，即能以理論計算出待量測之群速度色散係數大小。

ABSTRACT

Title：New group velocity dispersion measurement technique by using periodic wavelength-scanning pulse light source

Pages：1 Page

School：National Chiao Tung University

Department：Institute of Electro-Optical Engineering

Time：June, 2009 Degree：Master

Researcher：Shiou-Fong Liu Advisor：Prof. Yin-Chieh Lai

Group velocity dispersion (GVD) plays an important role in many applications such as high speed communication, nonlinear optics, ultrafast optical processing and other scientific researches. A new Group velocity dispersion (GVD) measurement method has been reported and demonstrated by using a periodic wavelength-scanning pulse source such as an asynchronously modelocked Er-fiber soliton laser or a frequency-shift keying (FSK) modulation light source with a RF spectrum analyzer. In the experimental work of the thesis, an asynchronous mode-locked fiber soliton laser has been used as the main light source. The laser was previously developed in our lab and is with some interesting properties including the slow periodic variation of the pulse timing position variation and the pulse central wavelength. By observing the pulse timing position variation of the pulse train before and after test fiber with the use of a RF spectrum analyzer, the group velocity dispersion of the test fiber can be inferred from the theoretical formula.

Acknowledgments

在碩士生涯中，首先要特別對我的指導教授 賴暎杰老師在研究的過程中不斷的給予支持與耐心的指導表達敬意與感謝之意，使我在求學的過程中受益良多，而老師的待人處世，更是值得我效仿學習。實驗方面特別感謝鞠曉山學長教導我許多實驗的方法及報告技巧，無私的指教與修正了我許多理論觀念，如果沒有學長如此的耐心指導下這篇論文無法如此順利產生。

此外特別要感謝 項維巍學長，平時在實驗方面給予方向的指導與做實驗期間細心和不厭其煩的教導，並適時給我鼓勵打氣。感謝 林俊廷學長、徐桂珠學姐、許宜蓁學姐、施伯宗學長、江文智學長和吳芳銘學長在課業和實驗上的指教。感謝張宏傑學長指導我許多的實驗技巧，提供不少實驗上面的幫助。

接下來感謝實驗室的同學昱勳、子翔、佩芳、小咨、漢昇、士愷、昱宏，與他們的交討與討論，讓我在課業上、實驗上，與相關領域的了解，獲益匪淺，以及在生活上彼此的幫忙照應；感謝學弟妹 家豪、柏萱、柏崴、姿媛等人的熱情支持與打氣，讓我在實驗室生涯中增添色彩。感謝實驗室的大家，除了在課業方面的幫助外，一起運動，出遊，共同歡笑回憶滿滿的豐富了碩士生活，同時也謝謝所有幫助過我的人。

最後要感謝我的父母和家人在我挫折的時候依然支持我，用你們的方式鼓勵著我，讓我能順利的完成碩士學業。而父母從小的關愛和照顧，是我永難回報的。

CONTENTS

LIST OF FIGURES

LIST OF TABLE

Chapter 1

Introduction

1.1 Overview

Group velocity dispersion (GVD) is the effect that the group velocity of light inside a propagation medium is wavelength dependent. One consequence of the GVD is the pulse broadening effect which arises from the wavelength-dependent time delay of different frequency components. The GVD can limit the maximum data rate or transmission distance in optical transmission due to adjacent signal overlap caused by pulse broadening. Hence the GVD plays an important rule in many applications including fiber communication, nonlinear fiber optics and ultrafast fiber optics. In the literature, several dispersion measurement methods have been proposed and demonstrated. These include the modulation phase-shift (MPS) technique [1], time of flight (TOF) technique [2], temporal interferometry method [3], spectral interferometry method [4], and soliton-compression method [5].

The MPS technique is by measuring the modulation phase variation of the transmitted amplitude-modulated signal. The TOF technique is by measuring the delay time between adjacent wavelengths with the use of fast PDs and oscilloscopes directly. The principles of the interferometry method and the spectral interferometry method are to measure the phase difference induced by the time delay between the reference fiber and the test fiber with an interferometer, like an Mach-Zehnder interferometer. The soliton-compression method measures both the value of the second-order dispersion coefficient and the nonlinear coefficient in optical fibers. This method is based on the

higher-order soliton pulse compression phenomenon and is valid for dispersion values greater than 0.5 ps/km/nm. Due to the issues of configuration complexity, environmental stability and measurement sensitivity, the modulation phase-shift (MPS) technique is probably the most widely used method in practice. However, since the method requires the phase measurement of a high frequency RF modulation signal, expensive equipments like a network analyzer are typically needed.

1.2 Motivation

In the thesis, we propose and demonstrate a new method of group velocity dispersion measurement just based on a swept-wavelength pulse light source and a RF spectral analyzer. This dispersion measurement system is not only with a simple configuration but also with economic advantages because the RF spectral analyzer is cheaper than the network analyzer used in the typical MPS system. In this method, a frequency-swept pulse source (i.e., an asynchronously modelocked Er-fiber soliton laser with sinsousoidal frequency modulation or a binary frequency-shift-keying (FSK) pulse light source) can be used as the input light source. The asynchronously modelocked Er-fiber soliton laser (ASM) we proposed previously has some interesting dynamic characteristics. One of the critical characteristics related to dispersion measurement is the slow periodic central frequency variation. In the proposed dispersion measurement method, the ASM light source will induce an extra slow periodic pulse timing position variation through the dispersion effect of the test fiber. By measuring the periodic pulse timing position variation before and after connecting the test fiber through the RF spectral measurement, the fiber dispersion can be readily determined. In

principle, a similar procedure can be carried by using a FSK light source to determine the dispersion with slightly different theoretical formula.

1.3 Thesis organization

This thesis is consisted of four chapters. Chapter 1 is an overview of the GVD measurement methods and our motivation for doing this research. Chapter 2 is the theory of the new GVD measurement method derived form the ASM laser dynamics. Chapter 3 presents the experimental setup and the measurement results to demonstrate the feasibility of the new dispersion measurement method. Finally Chapter 4 gives a summary about the obtained results and discuss possible future work.

Reference

[1] L. G. Cohen, “Comparison of Single-Mode Fiber Dispersion Measurement Techniques,” IEEE J. Lightw. Technol, vol. LT-3, pp. 958–966, 1985.

[2] J. M. Wiesenfeld and J. Stone, “Measurement of Dispersion Using Short Lengths of an Optical Fiber and Picosecond Pulses from Semiconductor Film Lasers,” IEEE J. Lightw. Technol, vol. LT-2, pp. 464–468, 1984.

[3] C. Palavicini, Y. Jaouën, and G. Debarge, “Phase-sensitive optical low-coherence reflectometry technique applied to the characterization of photonic crystal fiber properties,” Opt. Lett. vol. 30, pp. 361 – 363, 1984.

[4] P. Merritt, R. P. Tatam, and D. A. Jackson, “Interferometric Chromatic Dispersion Measurements on Short Lengths of Monomode Optical Fiber,” Opt. Lett., vol. 7, pp. 703-716, 1989.

[5] T. N. Nguyen, T. Chartier, M. Thual, P. Besnard, L. Provino, A. Monteville and N. Traynor, “Simultaneous measurement of anomalous group-velocity dispersion and nonlinear coefficient in optical fibers using soliton-effect compression,” Opt. Commun., vol. 278, pp. 60-65, 2007.

Chapter 2

Theories of the new GVD measurement method

2.1 Theory of ASM modelocking

For many applications of high speed fiber communication[1] and the ultrafast optical processing[2-3], a modelocking fiber laser that can directly output ultrashort (< ps) pulses at a very high repetition rate (>= 10GHz) [4-6] is very advantageous but challenging to achieve. Compared to the traditional modelocking techniques, asynchronous soliton modelocking (ASM) has the benefit to provide a good solution for related issues due to the employed hybrid modelocking effects. In an asynchronous soliton modelocking laser, the deviation frequency, (i.e., the difference between the modulation frequency and the cavity harmonic frequency), is not zero but is about several kHz to tens kHz. The soliton pulses can react against the frequency shift caused be the modulation frequency deviation and still remain stable mode-locking with a short pulsewidth (<1ps). Moreover, by asynchronous operation the laser noises will also be reduced through the equivalent sliding-filter effect at each roundtrip and the supermode suppression ratio (SMSR) of the laser can be smaller than -70dBm[7]. Most interestingly, the ASM laser exhibits slow periodic variation of the output pulses parameters as will be explained in more details below.

2.1.1 Master equation of ASM modelocking

Under the small roundtrip change assumption, an asynchronously modelocked fiber soliton laser can be described by the master equation as follows: [8] [9]

$$\frac{\partial u(T,t)}{\partial T} = \left(\frac{g_0}{1+\frac{\int |u|^2\, dt}{E_s}} - l_0\right)u + (d_r + jd_i)\frac{\partial^2 u}{\partial t^2} + (k_r + jk_i)|u|^2 u + jM\cos[\omega_m(t+RT)]u. \tag{2.1}$$

Where $u(T,t)$ is the complex field envelope of the pulse, g_0 is the unsaturated gain, E_s is the gain saturation energy, l_0 is the linear loss, d_r represents the effect of the optical filtering, d_i is group velocity dispersion, k_r represents the effect of equivalent fast saturable absorption caused by the polarization additive pulse modelocking (P-APM), k_i is the self phase modulation coefficient, M is the phase modulation strength, ω_m is the angular modulation frequency, T is the number of the cavity round trip, t is the time axis measured in the moving frame propagating at a specific group velocity along with the pulse, and R is the linear timing walk-off per roundtrip due to asynchronous phase modulation, which can be expressed by

$$R = N\left(\frac{1}{Nf_R} - \frac{1}{f_m}\right) = \frac{\delta f}{f_R f_m}. \tag{2.2}$$

Here δf is the deviation frequency between the N-th cavity harmonic frequency Nf_R and the modulation frequency f_m. In the following analyses, the sinusoidal modulation curve of the phase modulator will be expanded by the Taylor's series at the center of the pulse $t_0(T)$ to the second order:

$$M\cos[\omega_m(t+RT)] \approx m_0 - m_1[t-t_0(T)] - m_2[t-t_0(T)]^2, \tag{2.3}$$

Where

$$m_1 = M\omega_m \sin\{\omega_m[t_0(T) + RT]\} \tag{2.4}$$

And

$$m_2 = \frac{M}{2}\omega_m^2 \cos\{\omega_m[t_0(T) + RT]\}. \tag{2.5}$$

Such an approximation should be quite accurate since the laser pulsewidth is much shorter than the modulation time period in modelocked fiber lasers.

2.1.2 Variational analysis of ASM

The master equation (2.1) describing ASM can be reformulated as a variational problem and then solved approximately by assuming a reasonable pulse solution ansatz [10]. In the variational approach, the Lagrangian corresponding to the master equation (2.1) is

$$\begin{aligned} L = {} & \frac{j}{2}(u\frac{\partial u^*}{\partial T} - u^*\frac{\partial u}{\partial T}) + d_i|\frac{\partial u}{\partial t}|^2 - \frac{k_i}{2}|u|^4 + jd_r(\frac{\partial^2 u_0}{\partial t^2}u^* - \frac{\partial^2 u_0^*}{\partial t^2}u) \\ & + j[k_r|u_0|^2 + (g - l_0)](u_0u^* - u_0^*u) + \{m_1(t - t_0[T]) + m_2(t - t_0[T] \end{aligned} \tag{2.6}$$

Where $g = \dfrac{g_0}{1 + \dfrac{\int |u|^2\, dt}{E_s}}$ is the saturated gain and the modulation curve has been expanded by (2.3)-(2.5). The master equation (2.1) can de derived from the Lagrange by taking the variation of the functional $I = \iint LdTdt$ with respective to u and u^*:

$$\delta I = \delta\iint L(u, u^*, \frac{\partial u}{\partial T}, \frac{\partial u^*}{\partial T}, \frac{\partial u}{\partial t}, \frac{\partial u^*}{\partial t})dTdt = 0, \tag{2.7}$$

which is equivalent to the following equation:

$$\frac{\partial L}{\partial u^*} = \frac{\partial}{\partial t}\frac{\partial L}{\partial(\frac{\partial u^*}{\partial t})} + \frac{\partial}{\partial T}\frac{\partial L}{\partial(\frac{\partial u^*}{\partial T})} \quad . \tag{2.8}$$

Note that the functions u_0 and u_0^* in equation (2.6) are treated like fixed functions so that they do not take part in the variational procedure in (2.7). However, they should be replaced by u and u^* respectively after performing the variation. This is the standard technique to deal with loss terms under the variational formulation, since all the non-conserved terms can not be directly handled in the usual Lagrangian formulation. For the ASM fiber lasers, the reasonable pulse solution ansatz [9] is given by

$$u(T,t) = a(T)\,\mathrm{sech}[\frac{t-t_0(T)}{\tau(T)}]^{1+j\beta(T)} e^{j[\omega(T)(t-t_0(T))+\theta(T)]}, \tag{2.9}$$

where $a(T)$ is the pulse amplitude, $\tau(T)$ is the pulsewidth, $t_0(T)$ is the pulse timing, $\beta(T)$ is the chirp, $\omega(T)$ is the pulse center frequency, and $\theta(T)$ is the phase. One can obtain the evolution equations of all the pulse parameters from the reduced Lagrange <L> :

$$\delta\int < L > dT = 0\,, \tag{2.10}$$

where

$$< L >= \int_{-\infty}^{\infty} L_{ansaltz}\, dt \tag{2.11}$$

and $L_{ansaltz}$ represents the Lagrange L in which the ansatz (2.9) has been substituted for the function u and u^*.

The evolution equations of the pulse parameters are derived from the corresponding Lagrange equations:

$$\frac{\partial < L >}{\partial x_i} = \frac{\partial}{\partial T}\frac{\partial < L >}{\partial(\frac{\partial x_i}{\partial T})}, \tag{2.12}$$

where x_i represents each pulse parameter in the ansatz (2.9). The final derived equations for the pulse center frequency, the timing, the chirp, the amplitude, and the pulsewidth are given below:

$$\frac{d\omega}{dT} = -m_1 - \frac{4d_r(1+\beta^2)}{3\tau^2}\omega \tag{2.13}$$

$$\frac{dt_0}{dT} = 2d_i\omega + 2d_r\beta\omega \tag{2.14}$$

$$\frac{d\beta}{dT} = \frac{m_2\pi^2\tau^4 + 2a^2\tau^2(k_i - k_r\beta) - 2(2d_i + d_r\beta)(1+\beta^2)}{3\tau^2} \tag{2.15}$$

$$\frac{da}{dT} = (g - l_0)a + \frac{a[8k_r a^2\tau^2 + 6d_i\beta - d_r(\beta^2 + 7 + 9\tau^2\omega^2)]}{9\tau^2} \tag{2.16}$$

$$\frac{d\tau}{dT} = -\frac{4(-2d_r + k_r a^2\tau^2 + 3d_i\beta + d_r\beta^2)}{9\tau} \tag{2.17}$$

For simplicity the evolution equation for the phase has been omitted because of irrelevance. Please also note that the linear timing drift effects caused by the asynchronous phase modulation are included in the expressions for m_1 and m_2 in (2.4) and (2.5), which are periodic functions of T and $t_0(T)$.

2.1.3 Periodic variation of the pulse parameters in ASM

The laser dynamics of ASM lasers can be investigated in terms of the evolution of the pulse parameters described by (2.13)-(2.17). To the lowest-order approximation, only the evolution of the pulse timing and the pulse center frequency are needed to be considered and the variation of all the other pulse parameters can be ignored. Equations (2.13) and (2.14) for chirpless pulse

($\beta = 0$) can be further simplified to the following two equations under the assumption that the oscillating pulse timing $t_0(T)$ is much less than the linear timing drift RT due to asynchronous modulation:

$$\frac{d\omega}{dT} = -M\omega_m \sin(\omega_m RT) - \frac{4d_r}{3\tau^2}\omega, \tag{2.18}$$

and

$$\frac{dt_0}{dT} = 2d_i\omega. \tag{2.19}$$

These two simplified coupled equations can also be derived from the soliton perturbation theory [8]. The solutions of (2.18) and (2.19) have the following forms:

$$\begin{aligned}\omega(T) &= \frac{M}{R}\frac{1}{\sqrt{1+(\frac{4d_r}{3\tau^2\omega_m R})^2}}\cos(\omega_m RT + \theta_d) \\ &= \Delta\omega\cos(2\pi\delta f TT_R + \theta_d)\end{aligned} \tag{2.20}$$

and

$$\begin{aligned}t_0(T) &= \frac{2d_i M}{\omega_m R^2}\frac{1}{\sqrt{1+(\frac{4d_r}{3\tau^2\omega_m R})^2}}\sin(\omega_m RT + \theta_d) \\ &= \Delta t_0 \sin(2\pi\delta f TT_R + \theta_d),\end{aligned} \tag{2.21}$$

Where the cavity roundtrip time T_R is the inverse of f_R, $\Delta\omega$ and Δt_0 are the half peak-to-peak displacements of the sinusoidal variation in the pulse center frequency and the pulse timing. The two solutions (2.20) and (2.21) indicate that to the lowest-order approximation the variation of the pulse timing and the pulse center frequency of ASM laser is simply sinusoidal at the deviation frequency δf. In addition, the phase difference between the pulse timing and the pulse center frequency is exactly $\pi/2$. This knowledge will be

utilized when we try to experimentally determine the pulse center frequency variation.

The accurate simulation results of the full set of coupled equations (2.13)-(2.17) are shown in Fig. 2.1. The simulation parameters used are given as follows: d_i =0.2, d_r =0.05, k_i =0.4, k_r =0.1, g_0 =4, l_0 =0.8, E_0 =0.47, M =0.8, f_R = 8 MHz, f_H =1250 f_R, and δf =25 kHz. These parameters are estimated by the following procedure. The units for time t is chosen to be 0.5 ps, which is of the same order with the laser pulsewidth. The value of d_r is then determined from the known filter bandwidth (13.5 nm) and the value of d_i is determined from the estimated cavity average dispersion (-4.1 ps^2 / km) as well as the cavity length (25 m). The values of l_0 and g_0 are from the roughly estimated loss and gain of the cavity. The values of k_i and k_r are estimated from the values of d_i and d_r under the assumption that the pulse is a chirpless fundamental soliton with roughly the unit normalized pulsewidth and the unit normalized amplitude. To be more specific, we have simply set $k_i = 2d_i$ and required $k_i : k_r = d_i : d_r$ [9]. The value of E_0 also can be estimated based on the above normalization assumption. The other parameters can be directly estimated from the actual experimental conditions. In this way, a reasonable set of parameters that correspond to the studied fiber laser can be obtained for illustrative studies. These numbers should not be very far from the actual operating conditions of the studied laser.

From the obtained plots, one can clearly observe the slow periodic variation at the deviation frequency as shown in Fig. 2.1 (a)–(d). The half peak-to-peak

displacement of the pulse center frequency variation is found to be ~125 GHz in Fig. 2.1(a), corresponding to the variation of the pulse center wavelength of 1 nm around central wavelength 1550 nm, and the half peak-to-peak displacement of the pulse timing is ~3 ps in Fig. 2.1 (b). Besides these two parameters, other pulse parameters are also found to exhibit smaller but more complicated slow periodic variation. In particular the evolution of the pulse amplitude and the pulse energy are shown in Fig. 2.1 (c) and Fig. 2.1(d) respectively, which clearly indicates that the oscillation is not purely sinusoidal and the components of the higher-order harmonics of the deviation frequency appear. Direct numerical simulation has also been performed to verify the obtained results and the excellent agreement between the variational approach and the direct numerical simulation has been found.

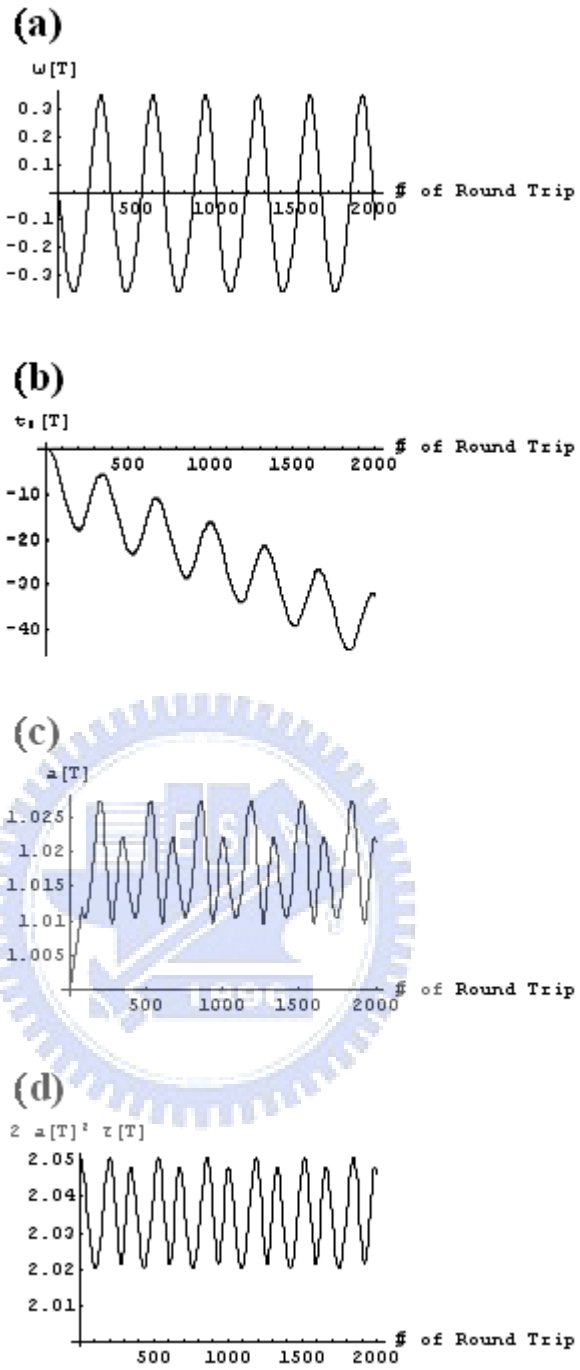

Fig. 2.1 Slow periodic evolution of the pulse parameters: (a) pulse center frequency; (b) pulse timing; (c) pulse amplitude; (d) pulse energy.

2.2 Sinusoidal swept-wavelength pulse light source

Different wavelength components will induce different time delays when the light propagates through the dispersive medium. In the proposed method we choose a swept-wavelength pulse light source to be the light source for the dispersion measurement. The asynchronously modelocked Er-fiber soliton laser exhibits the slow periodic swept-wavelength characteristics and thus is an ideal candidate. With the reasonable assumption that the pulse timing variation is mainly a simple sinusoidal function at the deviation frequency δf, the photocurrent from the fast photodiode detecting the pulse train can be expressed by

$$i(t) = [r(t) \otimes p(t)] \otimes \sum_{m=-\infty}^{m=\infty} \delta[t - mT_H + \Delta t_0 \sin(2\pi\delta f m T_H)], \tag{2.22}$$

where $r(t)$ is the response function of the fast photodiode, $p(t) = |u(t)|^2$ is the pulse intensity, $T_H = 1/f_H = 1/Nf_R$ is the period of the cavity harmonic, Δt_0 is the half peak-to-peak displacement of the sinusoidal pulse timing variation, $\delta(\cdot)$ is the Dirac's delta function, and $\otimes$ stands for the operation of convolution. The periodic pulse timing variation effect can be illustrated as in Fig. 2.2.

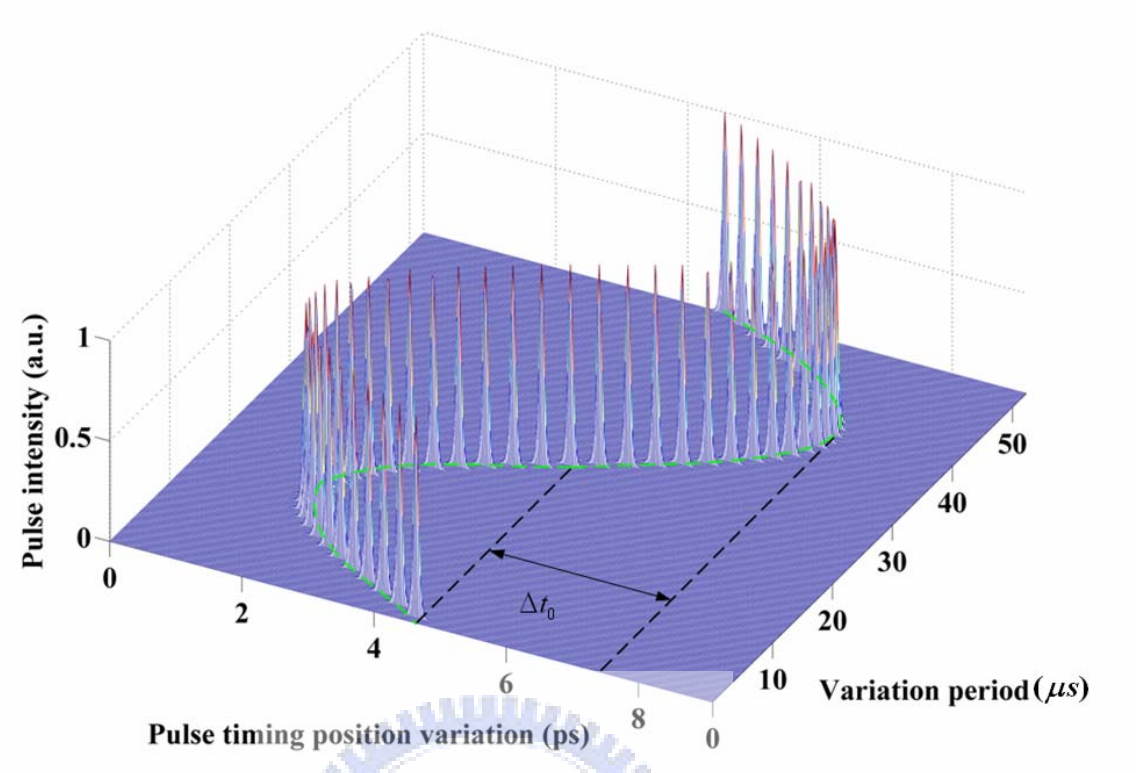

Fig. 2.2 The sinusoidal timing position variation

We have assumed that the variation of other pulse-shape parameters can be ignored at least to the first order approximation. This should be a reasonable assumption given with the theoretical results, where the variation of the pulse energy is much smaller in percentage. The Fourier transform of the photocurrent $i(t)$ can be expressed as:

$$I(\omega) \propto R(\omega)P(\omega) \sum_{m=-\infty}^{m=\infty} \sum_{n=-\infty}^{n=\infty} J_n(\omega \Delta t_0)\delta(\omega - 2\pi m f_H - 2\pi n \delta f), \quad (2.23)$$

where $R(\omega)$ and $P(\omega)$ are the Fourier transforms of the response function of the fast photodiode and the pulse intensity distribution respectively, and $J_n(\cdot)$ is the Bessel function of the first kind of order n. The periodic Dirac's delta functions with the sinusoidal timing variation in the time domain gives rise to the comb-like sub-components in the frequency domain as shown in Fig. 2.3. That is, the pure sinusoidal timing variation will produce the frequency

components with the amplitudes of $J_n(\omega\Delta t_0)$, which are spaced equally by the deviation frequency δf around the pulse train harmonics mf_H. When the pulsewidth is sub-ps short and the response speed of the photodiode is also fast enough compared to the slow modulation frequency, then the intensity of the n-th sub-component of $I(\omega)$ in (2.23) is simply proportional to $|J_n(\omega\Delta t_0)|^2$. Therefore by comparing the peak intensity at the main pulse train harmonic (n=0) to the peak intensity at the first sub-component (n=1) from the experimental data,

$$\Delta = \left| \frac{J_0[2\pi m f_H \Delta t_0]}{J_1[2\pi(mf_H + \delta f)\Delta t_0]} \right|^2 , \tag{2.24}$$

the half peak-to-peak displacement Δt_0 of the sinusoidal pulse timing variation can be identified

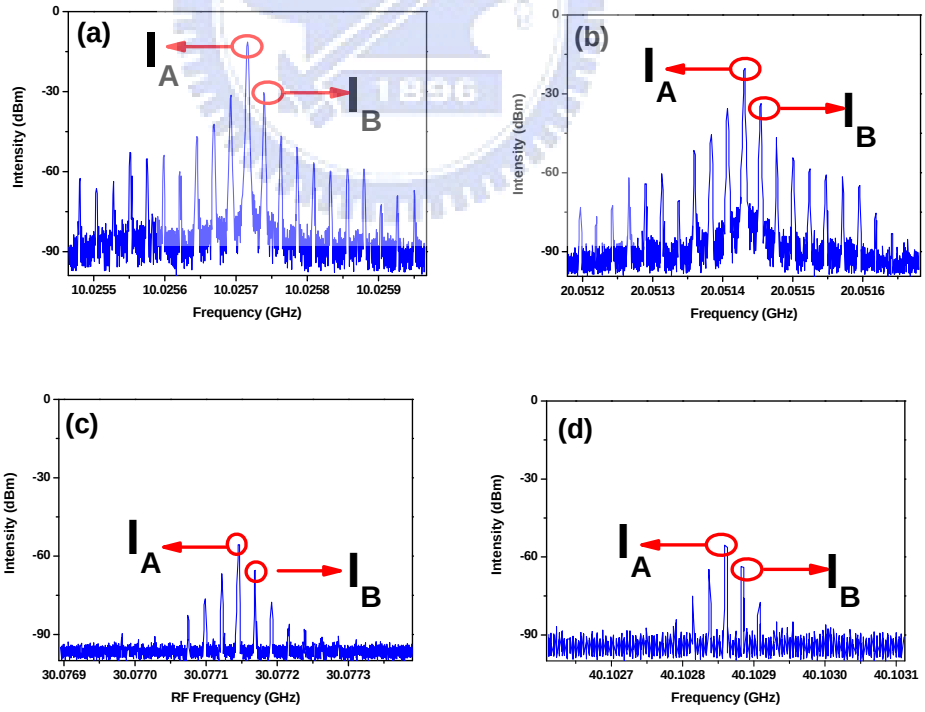

Fig. 2.3 RF spectra of the laser output with 500 kHz span. Data are taken (a) near 10 GHz; (b) near 20 GHz; (c) near 30 GHz; (d) near 40 GHz.

2.3 Experimental determination of the pulse timing variation by analyzing the RF spectra of laser output

Experimentally the peak intensity ratio Δ in (2.24) can be obtained directly by analyzing the RF spectra of the laser output. The output pulse train from the 10 GHz asynchronously mode-locked soliton Er-fiber laser is detected by a fast photodiode and the amplified electric signals of the photodiode are connected to a RF spectrum analyzer. The RF spectra with a smaller span of 500 kHz near the 10 GHz, 20 GHz, 30 GHz, and 40 GHz of the main pulse train harmonics have been shown in Fig. 2.3 (a)-(d) respectively. The values of the RF peak intensities I_A at mf_H and I_B at $mf_H + \delta f$ for m=1 to m=4 are represented by the solid squares in Fig. 2.4. According to (2.24), the differences between I_A and I_B are equal to

$$\begin{aligned} I_A - I_B &= 10\log_{10}\Delta \\ &= 20\log_{10}\left(\left|\frac{J_0[2\pi m f_H \Delta t_0]}{J_1[2\pi(mf_H+\delta f)\Delta t_0]}\right|\right) \\ &\approx 20\log_{10}\left(\left|\frac{J_0[2\pi m f_H \Delta t_0]}{J_1[2\pi m f_H \Delta t_0]}\right|\right). \end{aligned} \tag{2.25}$$

The fitting curve based on (2.25) shown by the solid line is used to identify the value of the half peak-to-peak displacement of the sinusoidal pulse timing variation Δt_0. The value is found to be around 3.5 ps for all the four values of m. The consistency of the estimated values from different orders of pulse train harmonics indicates that the proposed method should be able to give consistent and reasonable results for the pulse timing variation.

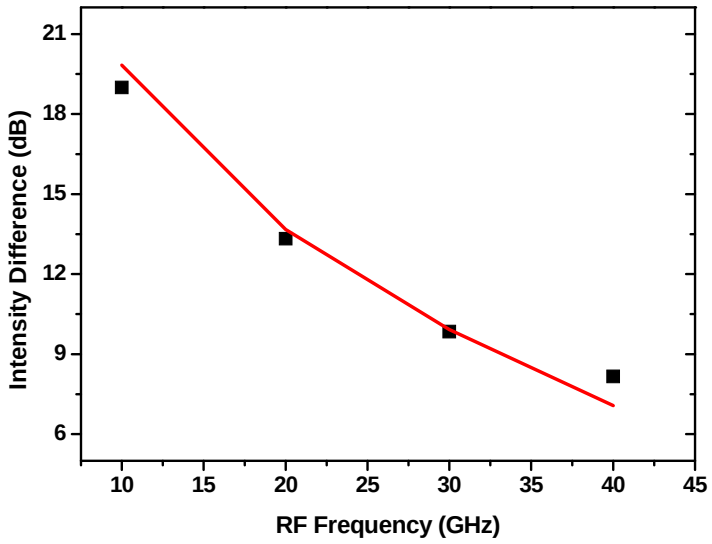

Fig. 2.4 Intensity difference between the 0th and 1st frequency subcomponents around the 10, 20, 30, 40 GHz pulse train harmonic frequencies.

2.4 Method to identify sinusoidal variation of pulse center frequency

The method developed above for determining the pulse timing variation can be further extended to identify the pulse center frequency (wavelength) variation as well. The pulse center wavelength variation will turn into extra pulse timing variation after the pulse train of ASM propagates through an external section of dispersive optical fiber. As indicated by (2.20) and (2.21), the phase difference between the two sinusoidal variations of the pulse timing and the pulse center frequency is $\pi/2$, i.e., sine and cosine respectively. Thus the variation of the pulse timing $\Delta t_1(T)$ of the ASM pulse train after propagating through a length L of the optical fiber with the dispersion parameter D will be given by:

$$\begin{aligned}\Delta t_{tot}(T) &= \Delta t_0 \sin(RT) + \Delta\lambda DL\cos(RT) \\ &= \sqrt{(\Delta t_0)^2 + (\Delta\lambda DL)^2}\sin(RT+\varphi) \\ &= \Delta t_1 \sin(RT+\varphi)\,,\end{aligned} \tag{2.26}$$

where $\Delta\lambda DL\cos(RT)$ is the extra pulse timing variation introduced by the dispersion of the external optical fiber. Based on (2.26), the half peak-to-peak displacement of the pulse center wavelength variation $\Delta\lambda$ can be determined according to

$$\Delta\lambda = \frac{\sqrt{\Delta t_1^{\,2} - \Delta t_0^{\,2}}}{DL} \tag{2.27}$$

with the additional experimental measurement for Δt_1 .

2.5 Binary frequency-shift-keying (FSK) pulse light source

Slow periodic frequency modulation produces slow periodic timing variation when the pulse train propagates in the dispersive test fiber. Through this effect the fiber GVD can be inferred accurately and sensitively. In principle, the frequency modulation format can be sinusoidal, binary-step-wise, or some other forms. Preliminary experimental demonstration has been achieved with an asynchronous modelocked (ASM) Er-fiber soliton laser and has been described in the previous sections [11-12], where the frequency modulation is sinusoidal. The possibility by using a binary frequency-shift-keying (FSK) pulse light source instead will be explored in the present section.

The pulse train with a periodic binary frequency modulation will experience a periodic pulse timing position modulation with only two different values. The Fig. 2.5 illustrates the single time delay difference of FSK signals without/with dispersion.

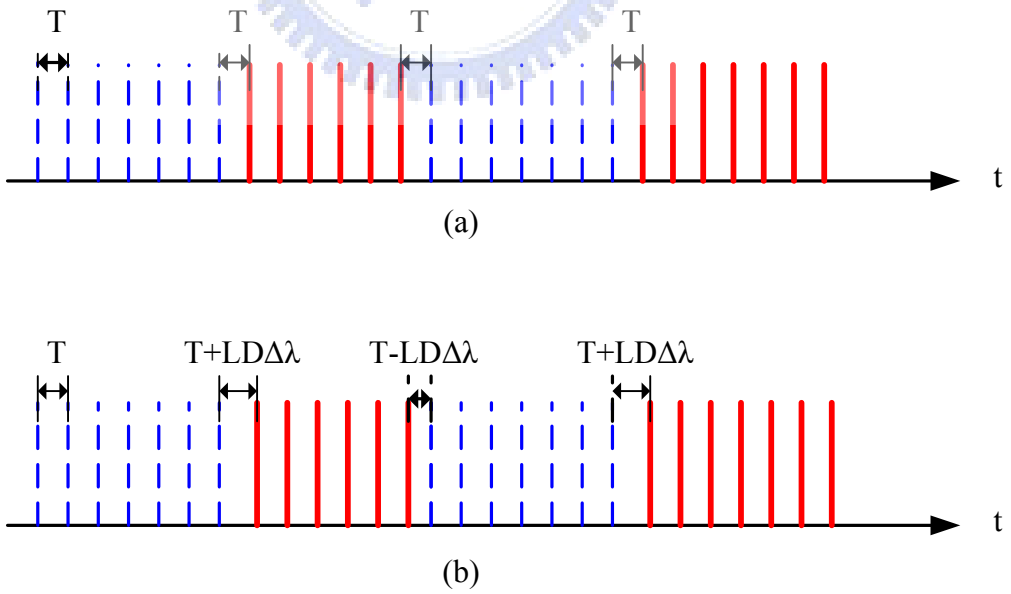

Fig. 2.5 The FSK pulse signals (a) without (b) with dispersion

By using the binary frequency-shift-keying modulation format as the example, the final detected signal can be written as:

$$f_{tot}(t) = m(t)\sum_{k=-\infty}^{\infty} f(t - kT_H) + [1 - m(t)]\sum_{k=-\infty}^{\infty} f(t - kT_H + DL\Delta\lambda)$$
$$m(t) = \begin{cases} 1 & 2n\pi \le \Omega t \le (2n+1)\pi \\ 0 & (2n+1)\pi \le \Omega t \le (2n+2)\pi \end{cases} \quad (2.28)$$

Here $f(t)$ is the detected signal of a single pulse, $m(t)$ is the signal for binary frequency-shift-keying, T_H is the timing period of the pulse train and $\delta t_0 = DL\Delta\lambda$ is the magnitude of the slow timing variation induced by the optical wavelength shift ($\Delta\lambda$) through the fiber GVD (D) with the fiber length (L). Finally Ω is the frequency of the binary frequency-shift-keying modulation. By carrying out the Fourier transform of $f_{tot}(t)$, it is not difficult to show that near the first harmonic component at $\omega_H = 2\pi / T_H$, the power ratio of the 0th (the cavity harmonic frequency) and 1st spectral side-peaks with a frequency separation of Ω can be written as:

$$\Delta \approx \frac{\pi^2}{4} \frac{1}{|\sin(\frac{\omega_H \delta t_0}{2})|^2} \quad (2.29)$$

This ratio values can be determined accurately from the experimental RF spectrum of the signals.

2.5.1 Principle of FSK

Frequency-shift keying (FSK) is a frequency modulation scheme in which digital information is transmitted through discrete frequency changes of a carrier wave. The simplest FSK is binary FSK (BFSK). BFSK literally implies using two discrete frequencies to transmit binary (0s and 1s) information. With this scheme, the "1" is called the mark frequency and the "0" is called the space frequency. The time domain of an FSK modulated carrier is illustrated in the Fig. 2.6.

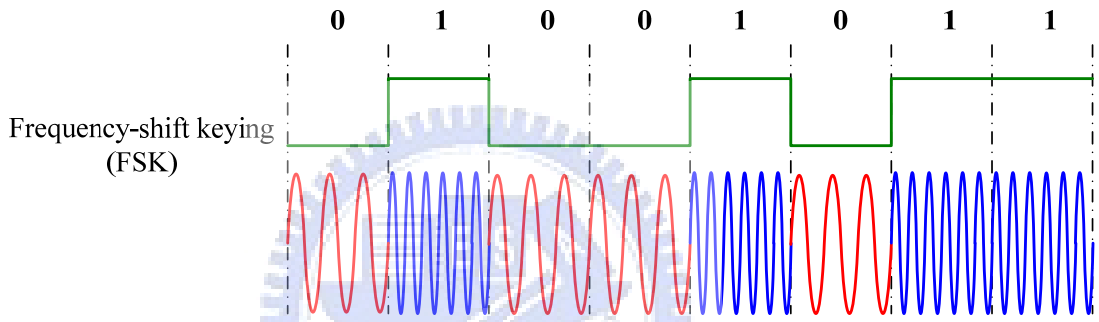

Fig. 2.6 Frequency-shifting keying modulation

The FSK signal can be generated by a FSK modulator consisted of two Mach-Zehnder Modulators (MZM) and a phase modulator. The Mach-Zehnder Modulator can be schematically illustrated in Fig.2.7.

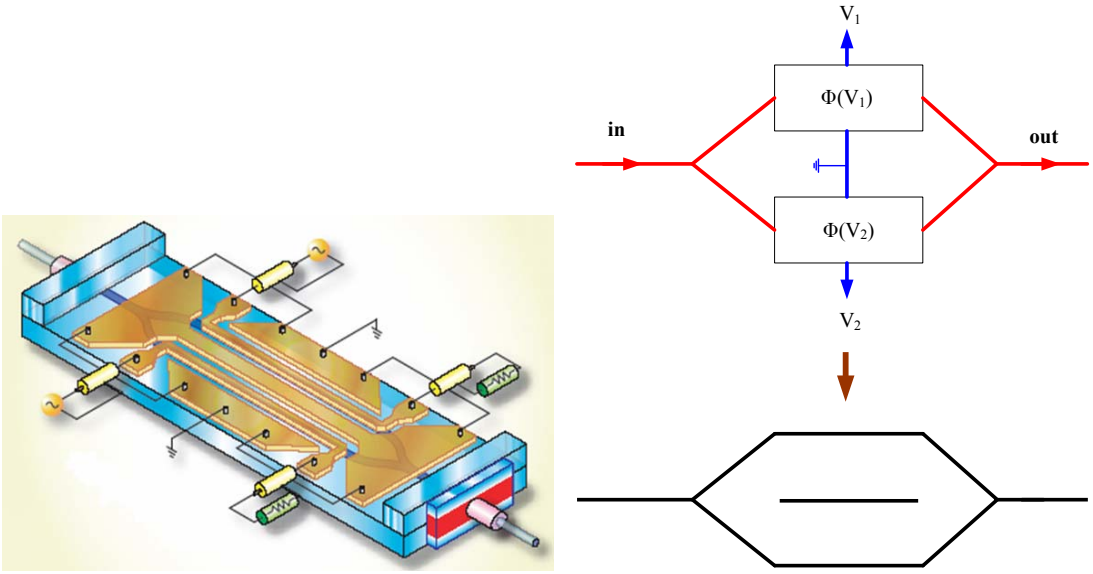

Fig. 2.7 Mach−Zehnder Modulator

The modulator has two waveguide arms with a phase modulator respectively and the refraction index is changed by the applied electric field. Then, the refraction index modulation gives rise to phase modulation and the modulator as a whole operates like an interferometer. If the phase difference between Φ(V1) and Φ(V2) is 180°, the output port sees destructive interference with no output light. On the contrary, if the phase difference between Φ(V1) and Φ(V2) is 0°, the output port see constructive interference with highest output light.

2.5.2 Operation of FSK

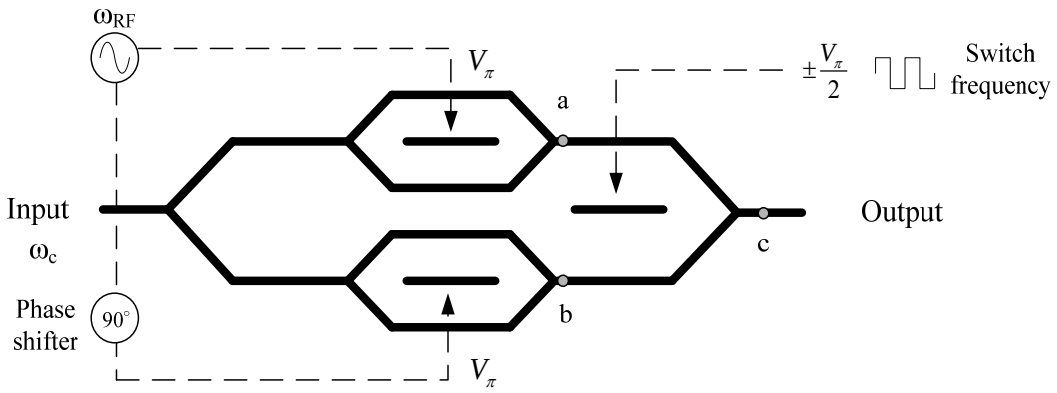

Fig. 2.8 FSK modulator

The layout of a FSK modulator can be shown as in Fig. 2.8. The input CW light has a carrier frequency ω_c. The frequency spectrum of "a" point has two peaks at $\omega_c - \omega_{RF}$ and $\omega_c + \omega_{RF}$ due to the amplitude modulation of the first modulator stage, which is illustrate by Fig. 2.9. Therefore, the main optical spectrum components to be considered are at ω_c, $\omega_c - \omega_{RF}$ and $\omega_c + \omega_{RF}$.

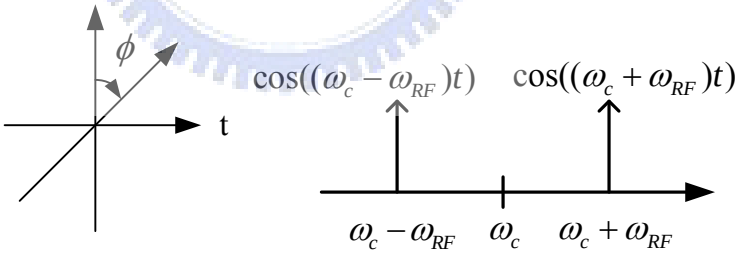

Fig. 2.9 The double side band

When we inject the modulation signal with a 90° phase shit to the Mach-Zehnder Modulator (MZM) in the bottom of Fig. 2.8, the phases of the spectral components will be different. The phenomenon is shown in Fig. 2.10.

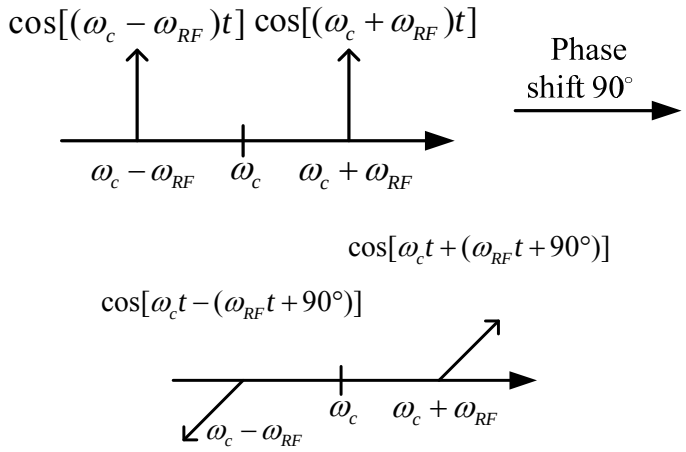

Fig. 2.10 Effects of the 90° phase shift

At the final stage of the modulator, the signals from two arms are added with a phase difference determined by the applied voltage of the modulator. When the modulation signal is at $\frac{V_\pi}{2}$, the spectrum is illustrated in Fig. 2.11. The signal at $\omega_c + \omega_{RF}$ will be totally suppressed by the 180° phase difference.

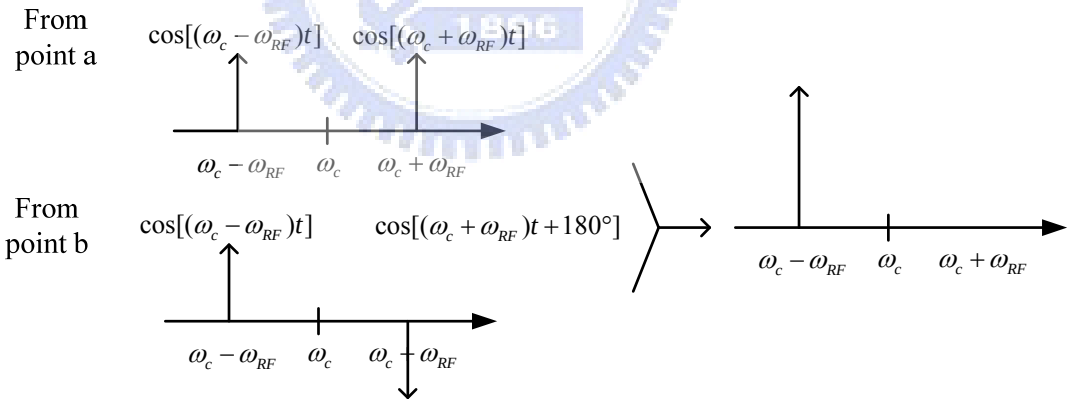

Fig. 2.11 Sideband at $\omega_c + \omega_{RF}$ is canceled

When the signal is at $-\frac{V_\pi}{2}$, the spectrum is illustrated in Fig. 2.12. This time the signal at $\omega_c - \omega_{RF}$ will be totally suppressed by the 180° phase difference.

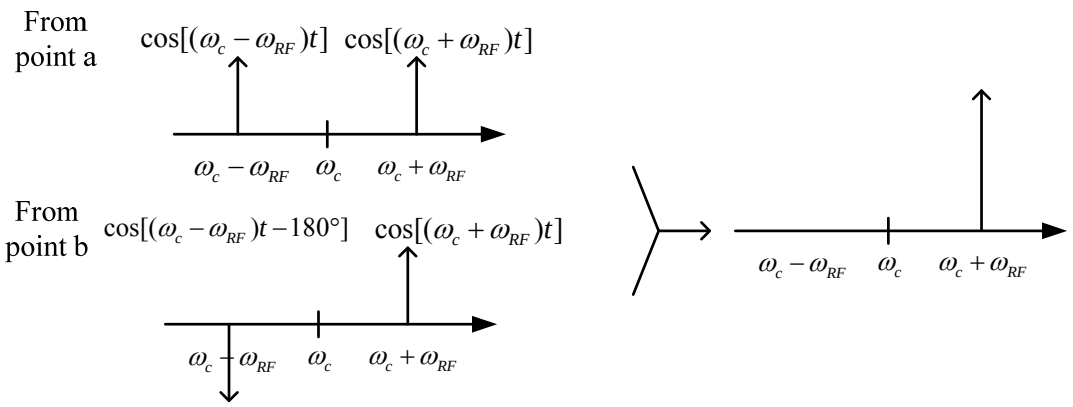

Fig. 2.12 Sideband at $\omega_c - \omega_{RF}$ is canceled

By the above operation method of FSK, we can get an output signal with double frequencies which can be switched in a controllable way [13].

Reference

[1] M. Nakazawa, H. Kubota, K. Suzuki, E. Yamada, and A. Sahara, "Ultra-high speed and long-distance TDM and WDM soliton transmission technology," IEEE J. Sel. Top. Quantum Electron., vol. 6, pp. 363-396, 2000.

[2] J. P. Wang, B. S. Robinson, S. A. Hamilton, and E. P. Ippen, "Demonstration of 40-Gb/s Packet Routing Using All-Optical Header Processing," IEEE Photon. Technol. Lett., vol. 18, pp. 2275-2277, 2006.

[3] Y. Miyoshi, K. Ikeda, H. Tobioka, T. Inoue, S. Namiki, and K. Kitayama, "Ultrafast all-optical logic gate using a nonlinear optical loop mirror based multi-periodic transfer function," Opt. Express, vol. 16, pp. 2570-2577, 2008.

[4] C. R. Doerr, H. A. Haus, and E. P. Ippen, "Asynchronous soliton mode locking," Opt. Lett., vol. 19, pp. 1958-1960, 1994.

[5] H. A. Haus, D. J. Jones, E. P. Ippen, and W.S. Wong, "Theory of soliton stability in asynchronous modelocking," IEEE J. Lightwave Technol., vol. 14, pp. 622-627, 1996.

[6] W.-W Hsiang, C.-Y Lin, M.-F Tien, and Y. Lai, "Direct generation of a 10 GHz 816 fs pulse train from an erbium-fiber soliton laser with asynchronous phase modulation," Opt. Lett., vol. 30, pp. 2493-2495 , 2005.

[7] J. N. Kutz, B. C. Collings, K. Bergman, W. H. Knox, "Stabilized pulse spacing in soliton lasers due to gain depletion and recovery," IEEE J. Quantum Electron., vol. 34, pp.1749-1757 ,1998.

[8] H. A. Haus, D. J. Jones, E. P. Ippen, and W.S. Wong, "Theory of soliton stability in asynchronous modelocking," IEEE J. Lightwave Technol., vol. 14, pp. 622-627, 1996.

[9] H. A. Haus, J. G. Fujimoto, and E. P. Ippen, “Structures for additive pulse mode locking,” J. Opt. Soc. Am. B, vol. 8, pp. 2068-2076 ,1991.

[10] D. Anderson, “Variational approach to nonlinear pulse propagation in optical fibers,” Phys. Rev. A, vol. 27, pp. 3135 – 3145, 1983.

[11] W.-W Hsiang, C.-Y Lin, M.-F Tien, and Y. Lai, “Direct generation of a 10 GHz 816 fs pulse train from an erbium-fiber soliton laser with asynchronous phase modulation,” Opt. Lett., vol. 30, pp. 2493-2495, 2005.

[12] W.-W. Hsiang, C. Lin, N. Sooi, and Y. Lai, “Long-term stabilization of a 10 GHz 0.8 ps asynchronously mode-locked Er-fiber soliton laser by deviation-frequency locking,” Opt. Express, vol. 14, pp. 1822-1828, 2006.

[13] S. Shimotsu, S. Oikawa, T. Saitou, N. Mitsugi, K. Kubodera, T. Kawanishi, and M. Izutsu, “Single Side-Band Modulation Performance of a LiNbO3 Integrated Modulator Consisting of Four-Phase,” IEEE Photon Tech. Lett., vol. 13, pp. 364-366, 2001.

Chapter 3

Experimental setup and results

3.1 The dispersion measurement system

The theory of our new dispersion measurement method has been explained in the previous chapter and in this chapter we will experimentally demonstrate the feasibility of the method. The pulse train from a wavelength-swept pulse light source will experience dispersion-induced periodic timing variation, which can be easily characterized by a RF spectrum analyzer. In this way the fiber GVD can be inferred accurately. The way of wavelength-sweeping can be sinusoidal, bi-wavelength sweeping, or some other sweeping formats. In this thesis work, the ASM is used as the sinusoidal format and FSK is used as the binary-step-wise format. The schematic setup of our proposed dispersion measurement system is shown in Fig. 3.1.

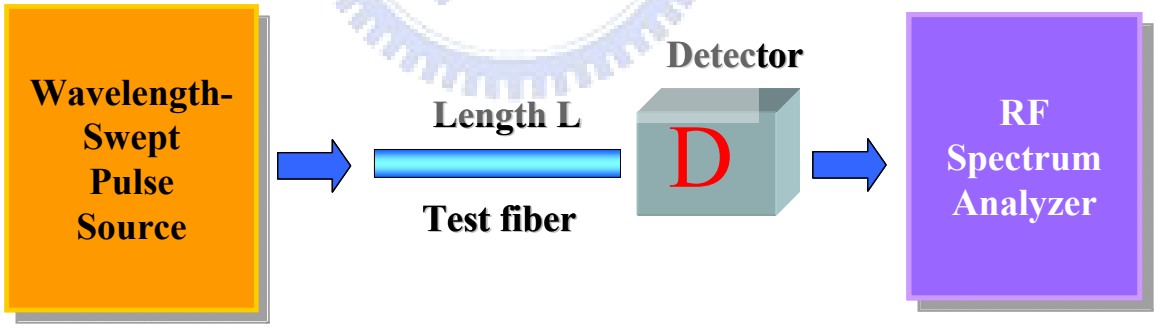

Fig. 3.1 Schematic setup of proposed dispersion measurement

3.2 The experimental setup with ASM laser source

The schematic setup of an asynchronous modelocked Er-fiber soliton laser is illustrated in Fig. 3.2.

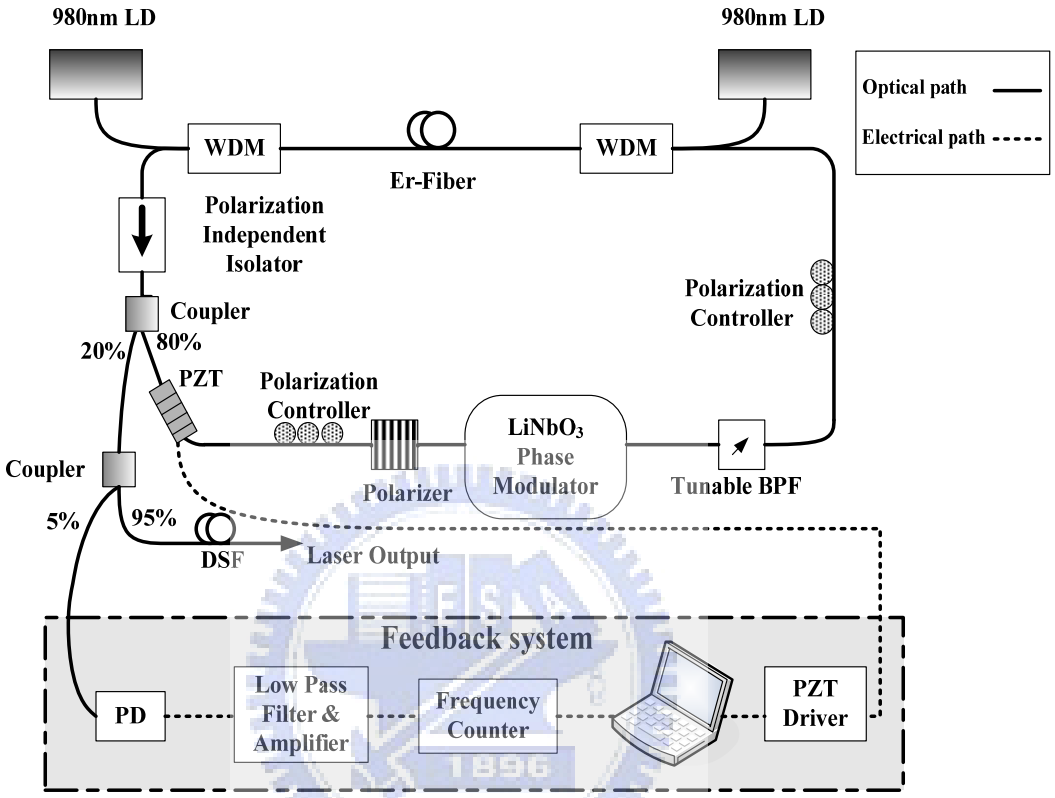

Fig. 3.2 Schematic setup of a 10GHz asynchronous modelocked Er-fiber soliton laser

In this laser, the technique of hybrid modelocking is used. We put an electro-optic modulators (EO) phase modulator into the cavity of a passive mode-locked laser and keep the setup all-fiber. The EO modulators can be constructed as integrated-optical devices. These devices operate at higher speeds and lower voltages than the bulk devices. The optical waveguide is fabricated on an electro-optics substrate (often $LiNbO_3$) by diffusing materials like titanium to increase the refractive index. The phase modulator needs a polarizer in the input

end to align the polarization axis of pulses with that of the EO crystal. The isolator is for single direction light propagation to prevent spatial hole burning. It is also polarization-independent since the polarizer and the phase modulator provides enough polarization dependent loss for achieving polarization additive pulse modelocking (P-APM). The two polarization controllers are placed in the cavity to adjust the polarization state for achieving P-APM. In order to get more nonlinearity in the fiber cavity, high intra-cavity light intensity is needed. As a result, the method of bi-directional pumping is utilized in the experimental setup and about 350 mW of 980 nm pump is used in the experiment. An EO phase modulator is put in the fiber ring cavity to achieve active mode-locking. If the EO modulator is replaced with a polarization dependent isolator, the laser becomes a purely passive mode-locked laser.

The tunable bandpass filter is used to select the lasing wavelength of the laser. In addition, it can cooperate with the self-phase modulation (SPM) effect in the cavity to suppress supermodes and to achieve a high supermode suppression ratio (SMSR). Besides, the wide bandwidth of the bandpass filter can support shorter pulses in the cavity so that the generated pulse width also can be shorter.

A section of 5.5 meters Erbium-doped fiber pumped by two 980 nm laser diodes acts as the gain medium of our laser. The output coupler is put behind the Er-fiber to get the greatest output power. The coupling ratio is 80/20 to couple 20% power inside the laser to the laser output. The chirp of the pulses is compensated with a length of negative group-velocity dispersion (GVD) fiber.

The feedback control circuit controlling the cavity length to lock the deviation frequency at a suitable value is used to stabilize the asynchronous mode-locked laser. The stabilization scheme is simple and economic due to the requirement of only electronics in the kHz range. It is composed of a photo

detector, a low pass filter, an amplifier, a frequency counter, a computer, a PZT driver, and a PZT. The signal obtained from the photo detector is amplified by the amplifier, and filtered out the unnecessary signals by the low pass filter. Then the signals we want are sent to the frequency counter connected to the computer. The PZT driver controlled by the LABVIEW software of the computer applies the voltage on the PZT, to change the cavity length for stabilizing the mode-locked laser. The devices that been used in the fiber ring cavity are list in table 3.1.

Table 3.1 The devices in the fiber ring cavity

1. 980nm pump laser : maximum output power : 602mA x 1 : 450mA x 1
2. EO phase modulator
3. Tunable bandpass filter: 3dB bandwidth: 13.5 nm ; central wavelength:1530~1570 nm
4. Polarization independent isolator x 2
5. WDM coupler (980 nm/ 1550 nm) x 2
6. PM fiber : located at the EO phase modulator
7. Erbium-doped fiber: about 5.5 M
8. Dispersion shifted singlemode fiber: about 2M
9. Single mode fiber: about 19.33 M
10. Coupler: 80/20 x 1; 95/5 x 1
11. Polarization controller x 2
12. Photo detector
13. Amplifier
14. Low pass filter: frequency 500 Hz to 64000 Hz

15. Frequency counter: frequency DC to 225 MHz
16. PZT driver: voltage 0 V to 150 V
17. PZT

The asynchronously modelocked Er-fiber soliton laser is basically a periodic sinusoidal wavelength-scanning pulse light source. The laser can provide the required center frequency variation $\Delta\lambda$ to induce pulse timing variation for the GVD measurement. The measurement is done in three steps. First we find the original pulse timing position variation δt_0 from the RF spectrum of the laser output. Then, we determine the center frequency variation $\Delta\lambda$ from calibrating with a SMF fiber which GVD and length has been known. Finally, we find the final pulse timing position variation δt_1 after the test fiber from the final RF spectrum. The GVD can then be determined from $\delta t_0, \delta t_1$, $\Delta\lambda$ and the fiber length L from Eq. (2.27). The system layout is shown as in Fig. 3.3.

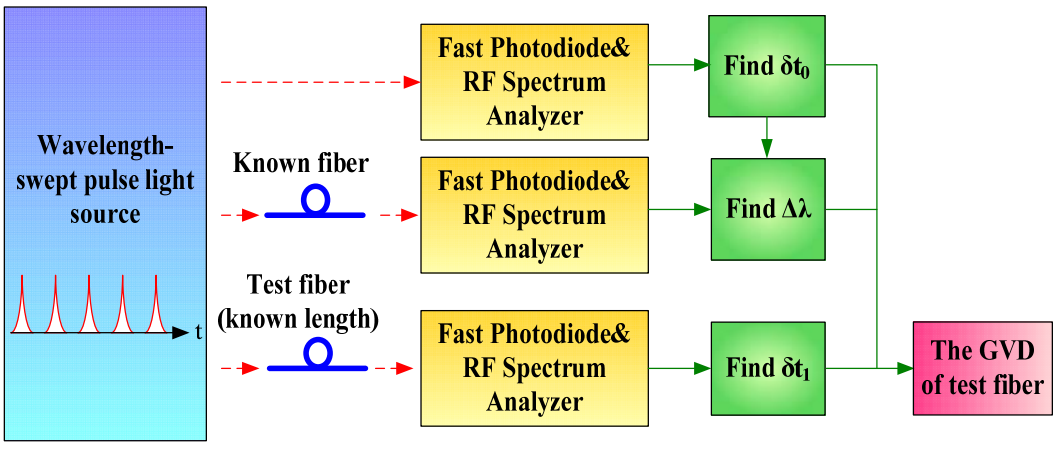

Fig. 3.3 Schematic setup of dispersion measurement

3.2.1 Result and analysis with ASM

The ASM laser source has some inherent periodical timing variation. When the laser light propagates through different type of fibers and length, additional periodical timing variation will be produced through the dispersion effect. A typical RF spectrum of the pulse train is shown in Fig.3.4. The magnitude of periodical timing variation will be changed by propagation but the frequency of periodical timing variation isn't changed. The value of frequency is 19k Hz and is called the detuning frequency (deviation frequency) of ASM fiber laser.

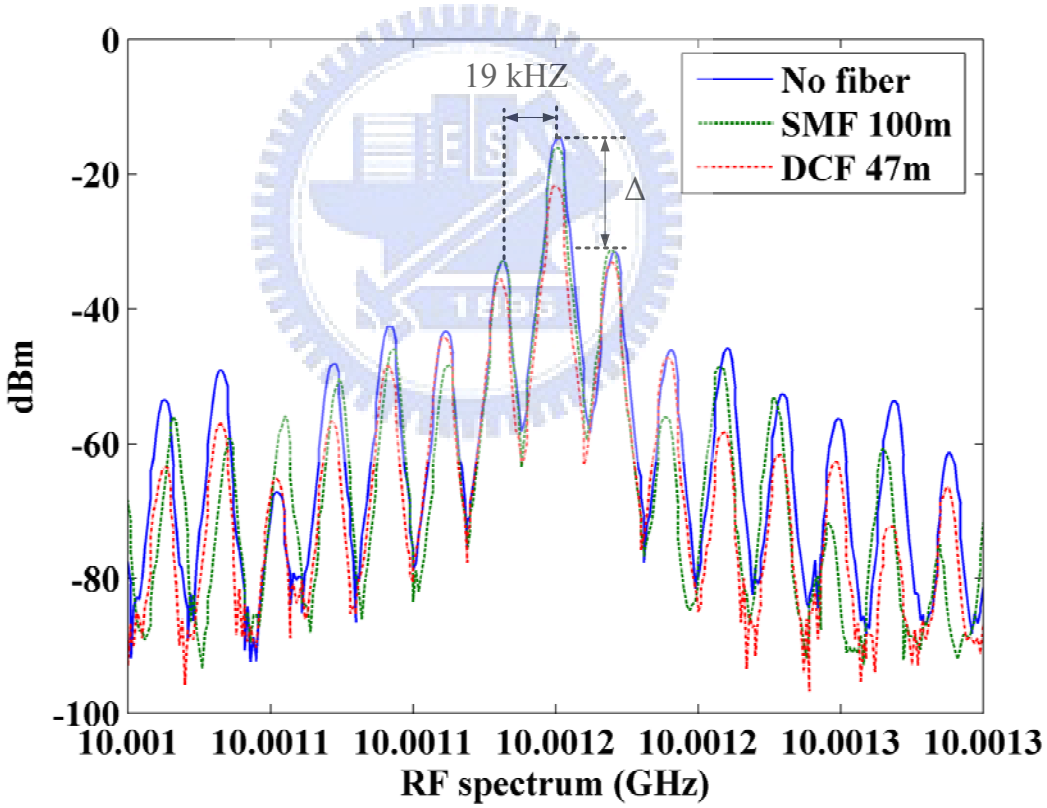

Fig. 3.4 The RF spectrum around the 10 GHz spectral harmonic

The central frequency (wavelength) variation of the pulse train can be determined by Eq. (2.27). The fitting curve is illustrated in Fig. 3.5. From the fitting the central wavelength variation value can be found.

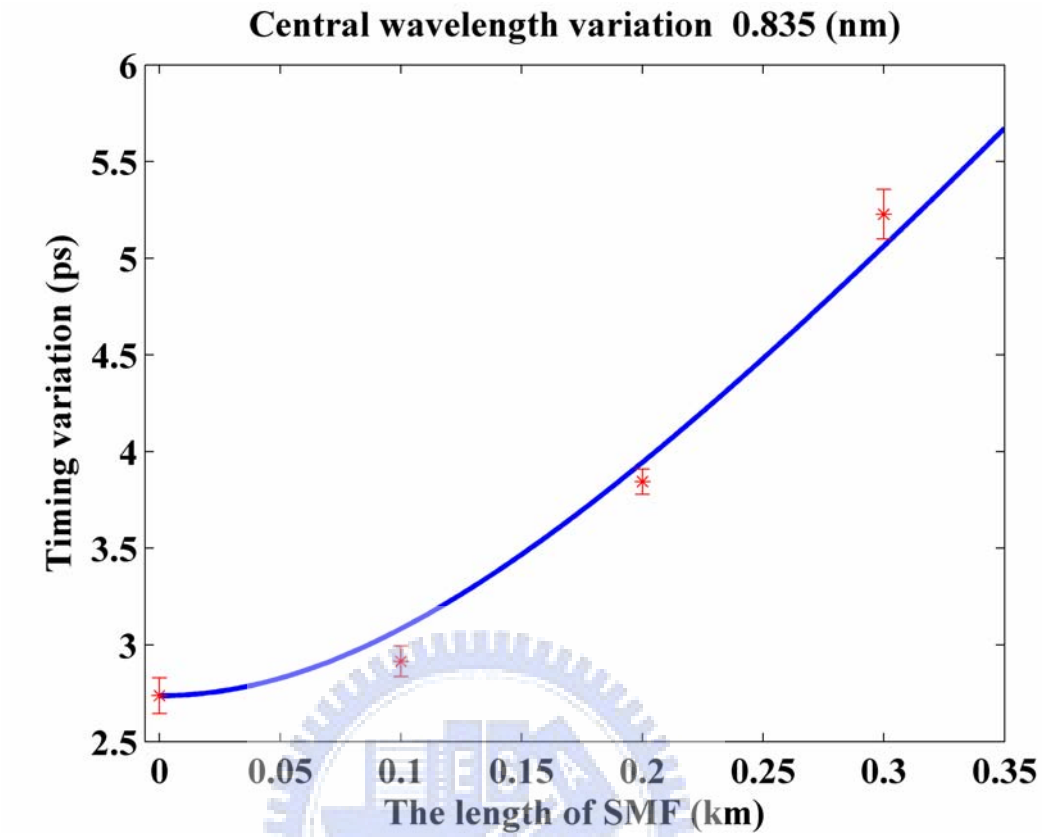

Fig. 3.5 The relation between the length of SMF and timing variation

The Fig. 3.6 one can see that different lengths of SMF will have different magnitudes of sub-spectral peaks. The tendency of the curves at shorter length of SMF reveals the limit on the small GVD value measurement. It is mainly due to the original timing position variation from the laser itself.

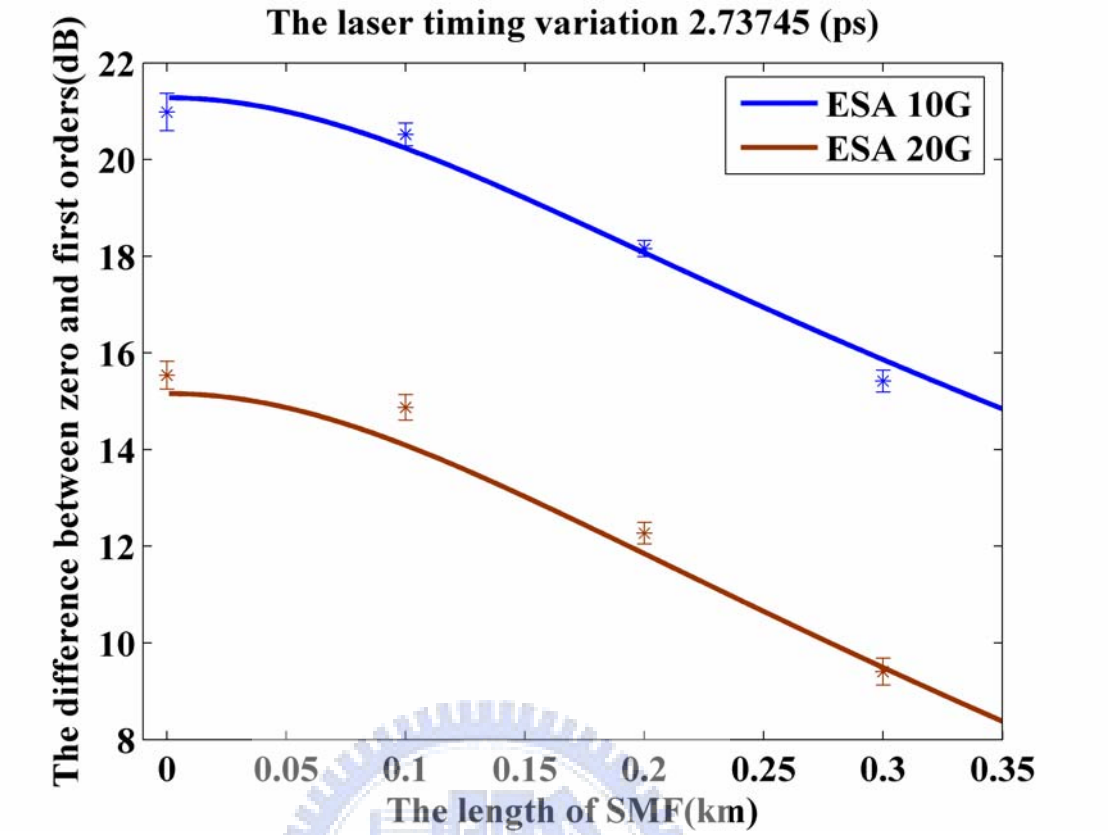

Fig. 3.6 The magnitude difference between zero and first order spectral peaks as a function of the fiber length

The results of GVD measurement are listed in Table 3.2. The GVD of a LEAF fiber and a DCF fiber are found to be 4.2 (ps/nm/km) and 111. (ps/nm/km) respectively. The central wavelength variation $\Delta\lambda$ is 0.835 (nm) and the timing position variation from laser source δt_0 is 2.74 (ps). The timing position variation δt_1 after connecting the test fibers (LEAF and DCF) are 3.05 (ps) and 5.16 (ps) respectively.

Table 3.2 Timing position variation and dispersion

Fiber type	Fiber length (m)	$\Delta\lambda$ (nm)	δt_{01} (ps)	δt_{02} (ps)	$\lvert D \rvert$ (ps/nm/km)
LEAF	380	0.835	2.74	3.05	4.2
DCF	47	0.835	2.74	5.16	111.

3.3 Simulation and experiment of FSK

As stated in the previous section, the critical limit with respect to the smallest GVD measurement is the original timing position variation δt_0 from the ASM laser source. In this section we try to build up a new measurement light source by CW light modulation instead of a pulse laser source. In this respect, the bi-wavelength sweeping light source is the simplest form to be tried. Thus we will use a FSK modulator and a Mach-Zehnder Modulator to carry out the new measurement source for replacing the ASM laser. In Fig. 3.7 we adopt an EO modulation scheme that is similar to the recently developed scheme for generating high frequency Radio-Over-Fiber vector signals [1]. The original timing variation should be zero or very small for this kind of frequency modulated pulse light source.

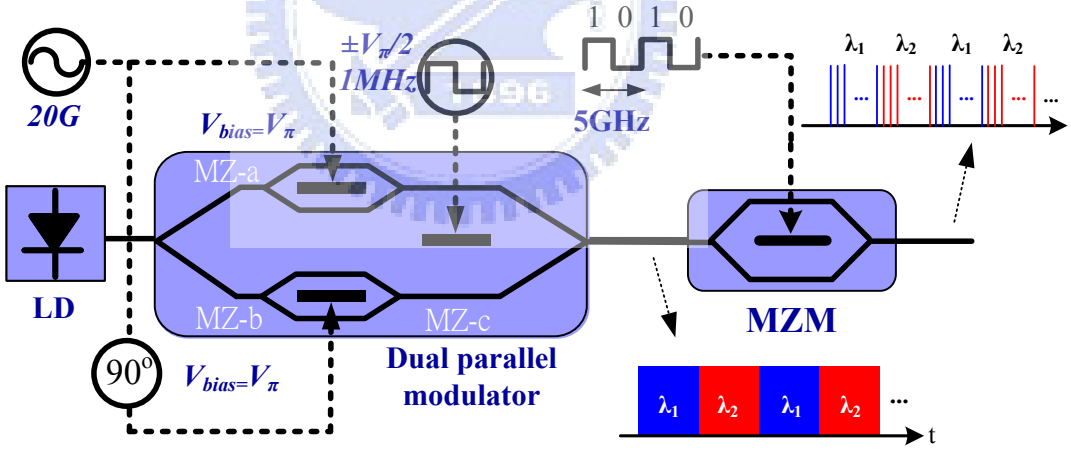

Fig. 3.7 FSK pulse light source

The system can be separated into three parts which are the light source, FSK modulator and Mach-Zehnder Modulator. The light source is a continuous wave laser (CW laser) at 1550nm which can be considered as a signal carrier. The FSK modulator can provide double frequency switch and the experimental measurement results are shown in Fig. 3.8, Fig. 3.9, and Fig.3.10.

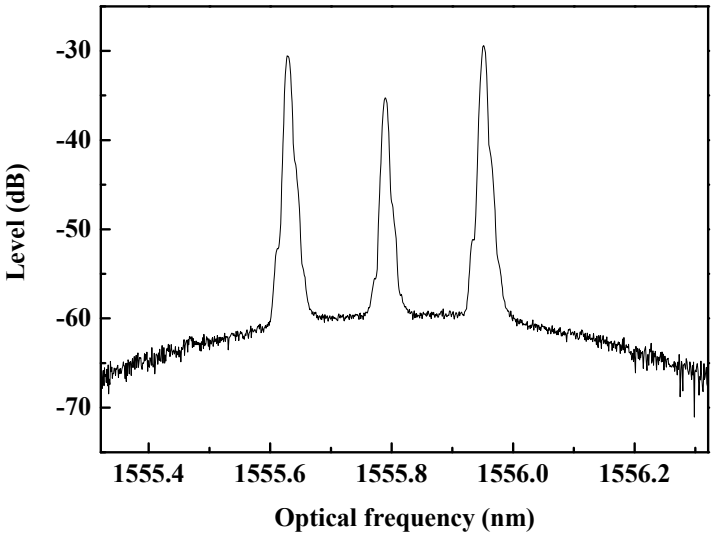

Fig. 3.8 Double sideband with FSK modulator

In the double sideband case, the central frequency is at 1555.8 nm, which is determined by the CW laser. The wavelength difference between the two double side peaks is 0.322 nm

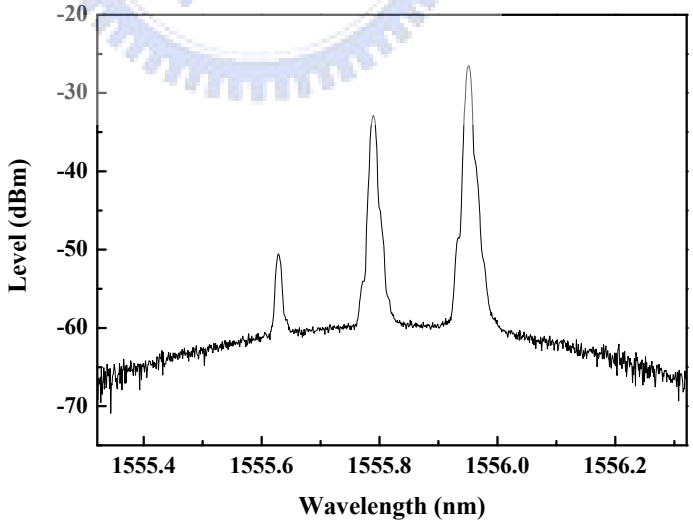

Fig. 3.9 Single sideband at 1555.951 nm

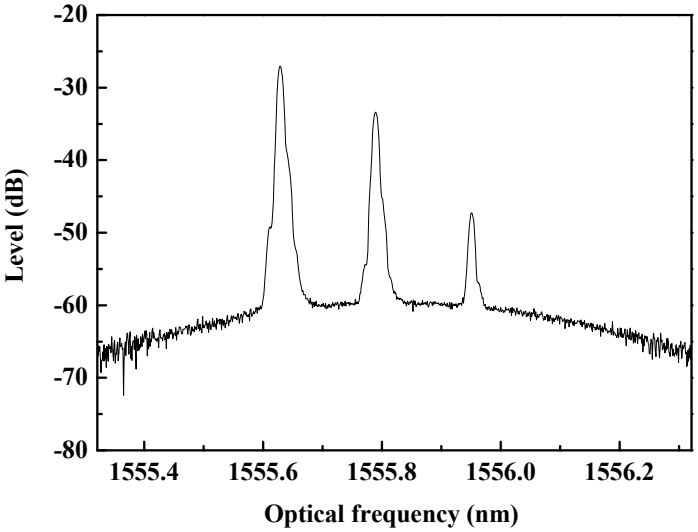

Fig. 3.10 Single sideband at 1555.951 nm

Then, the Mach-Zehnder Modulator driven by a pattern generator can produce 5G pulse trains. The optical spectra are in Fig. 3.11, Fig. 3.12 and Fig. 3.13.

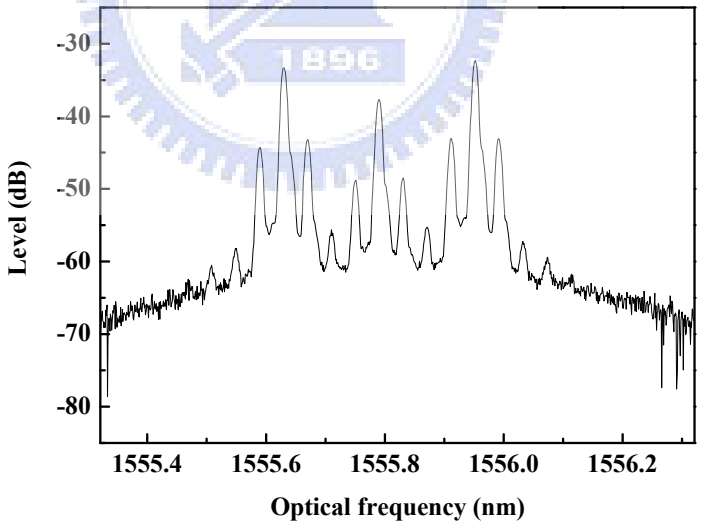

Fig. 3.11 Double sideband with FSK modulator and MZM

Compared with Fig. 3.8 we can see that extra side peaks are generated in Fig. 3.11. and the frequency difference is about 5GHz. Since the MZM will produce phase modulation.

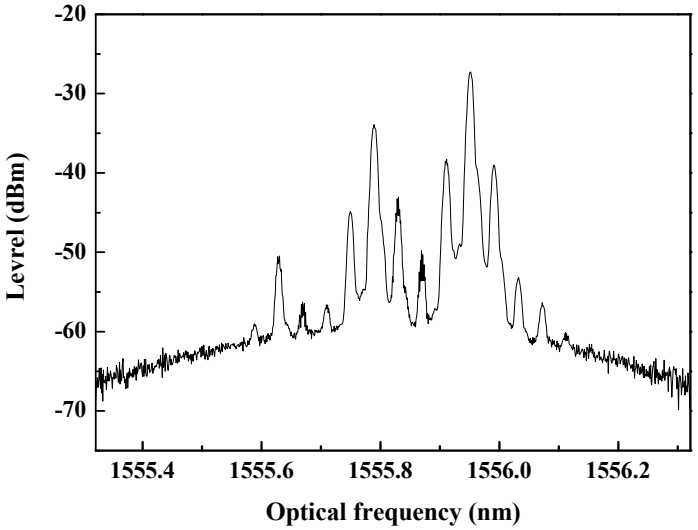

Fig. 3.12 Single sideband at right side with MZM

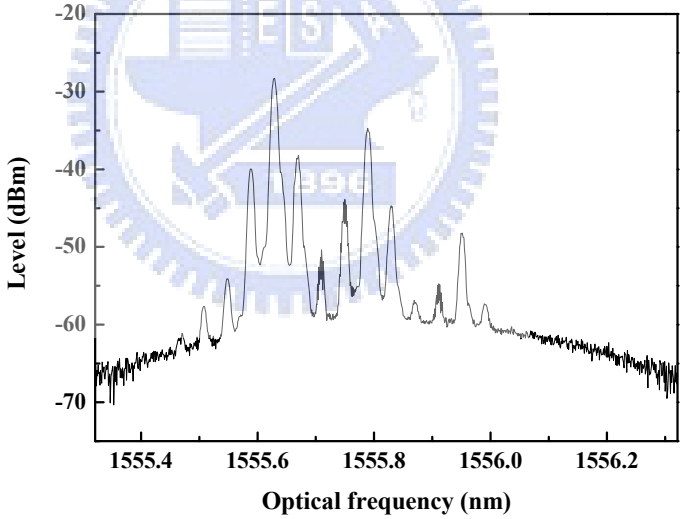

Fig. 3.13 Single sideband at left side with MZM

We have observed the RF spectra in 5GHz, 10GHz, 15GHz and 20GHz without connecting the test fiber respectively. The RF spectra are in Fig. 3.14, Fig. 3.15, Fig. 3.16 and Fig. 3.17.

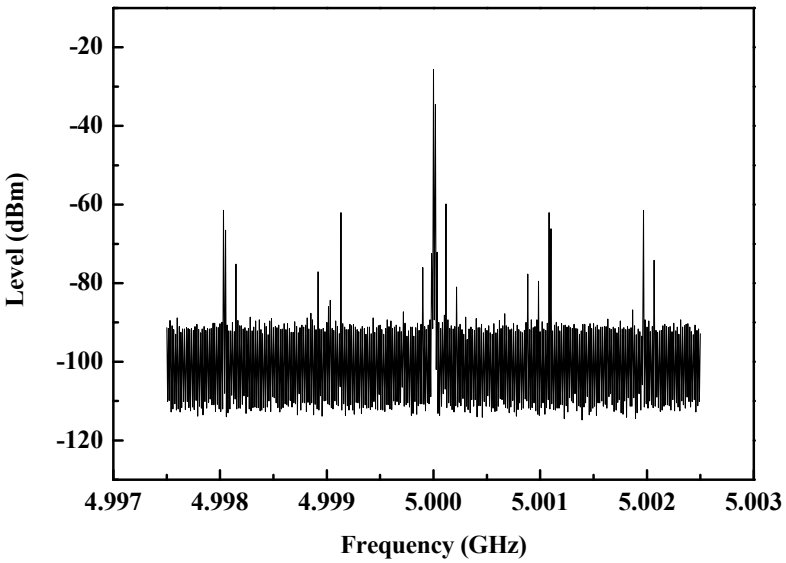

Fig. 3.14 RF spectrum at 5GHz without connecting fiber

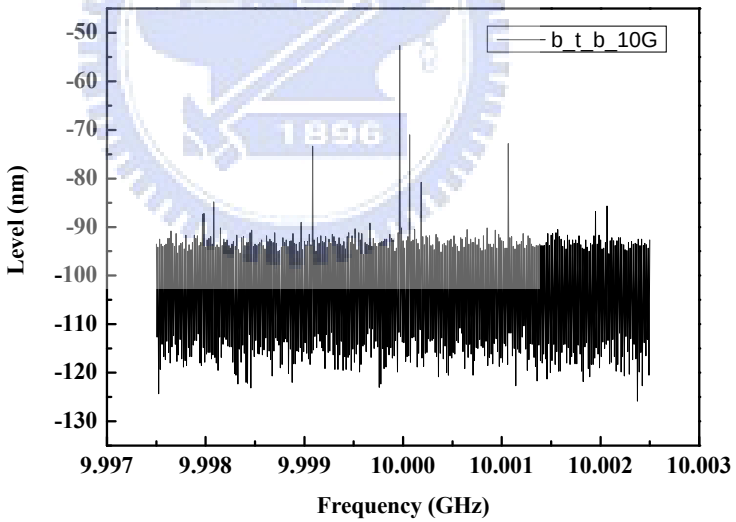

Fig. 3.15 RF spectrum at 10GHz without connecting fiber

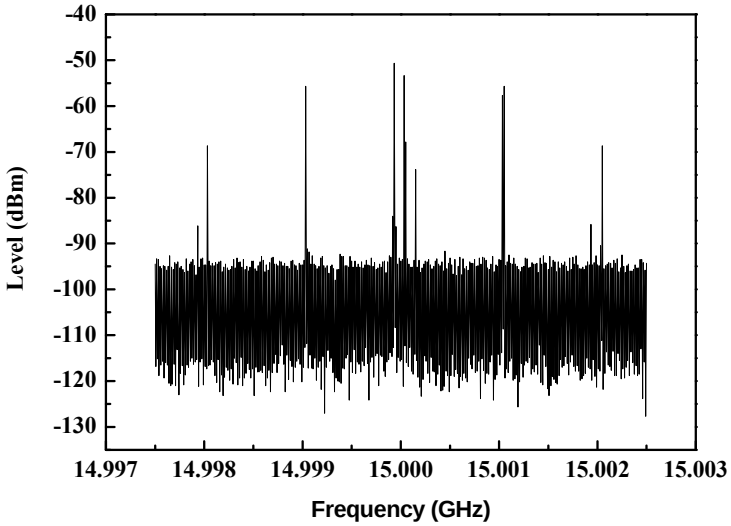

Fig. 3.16 RF spectrum at 15GHz without connecting fiber

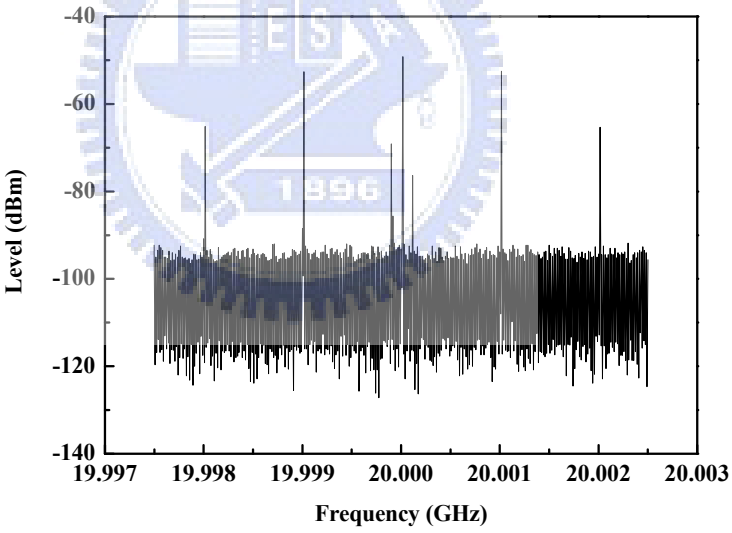

Fig. 3.17 RF spectrum at 20GHz without connecting fiber

From Fig. 3.14 to Fig.17, we can see four sidepeaks around the central frequency and the frequency difference between the peaks is 1MHz. There are some undesired sidepeaks in the figures. They may be due to the fact that the interference cancellation of the FSK modulator is not ideal and the fact that the central wavelength of the used tunable laser is drifting in time. One may be able

to select a more stable tunable laser and a more accurate band pass filter to solve the problem.

When the system is connected with a SMF fiber, the measurement figures are illustrated as Fig. 3.18, Fig. 3.19, Fig. 3.20 and Fig. 3.21.

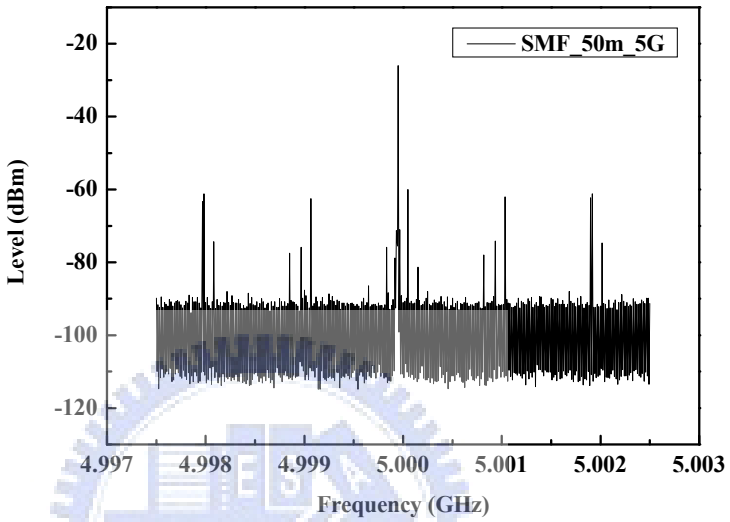

Fig. 3.18 RF spectrum at 5GHz with 50m SMF

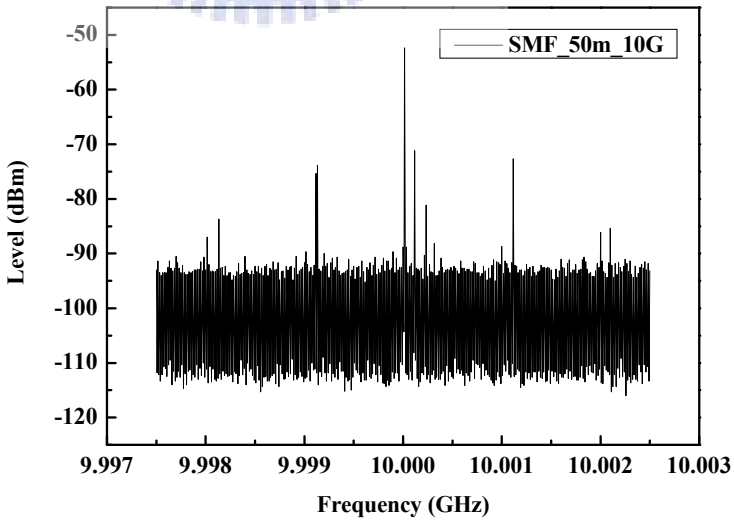

Fig. 3.19 RF spectrum at 10GHz with 50m SMF

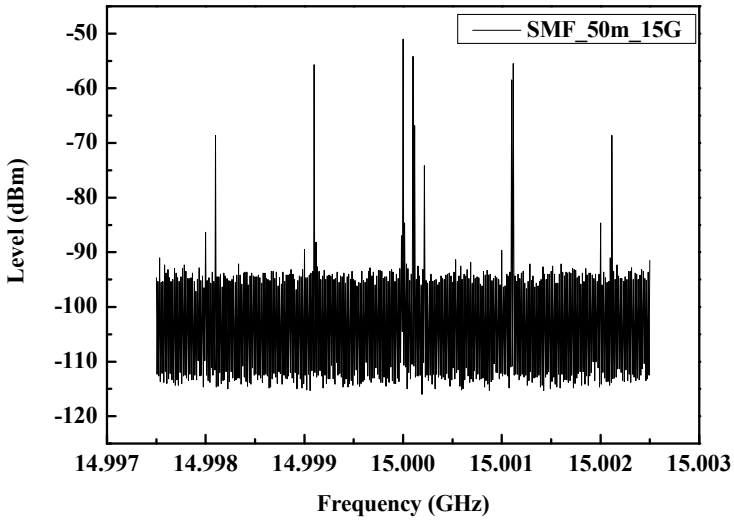

Fig. 3.20 RF spectrum at 15GHz with 50m SMF

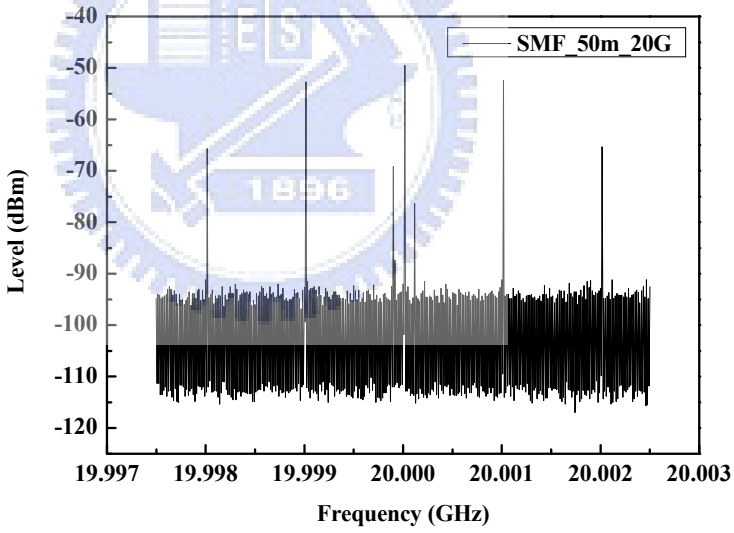

Fig. 3.21 RF spectrum at 20GHz with 50m SMF

When the light generated from the bi-wavelength sweeping light source goes through the test fiber, the GVD will cause sidepeaks around central frequency components. The relationship between the GVD and the magnitude ratio of sidepeaks has been derived in Eq. (2.29).

The measurement data can be compared with the analytic value and is

shown in Fig. 3.22.

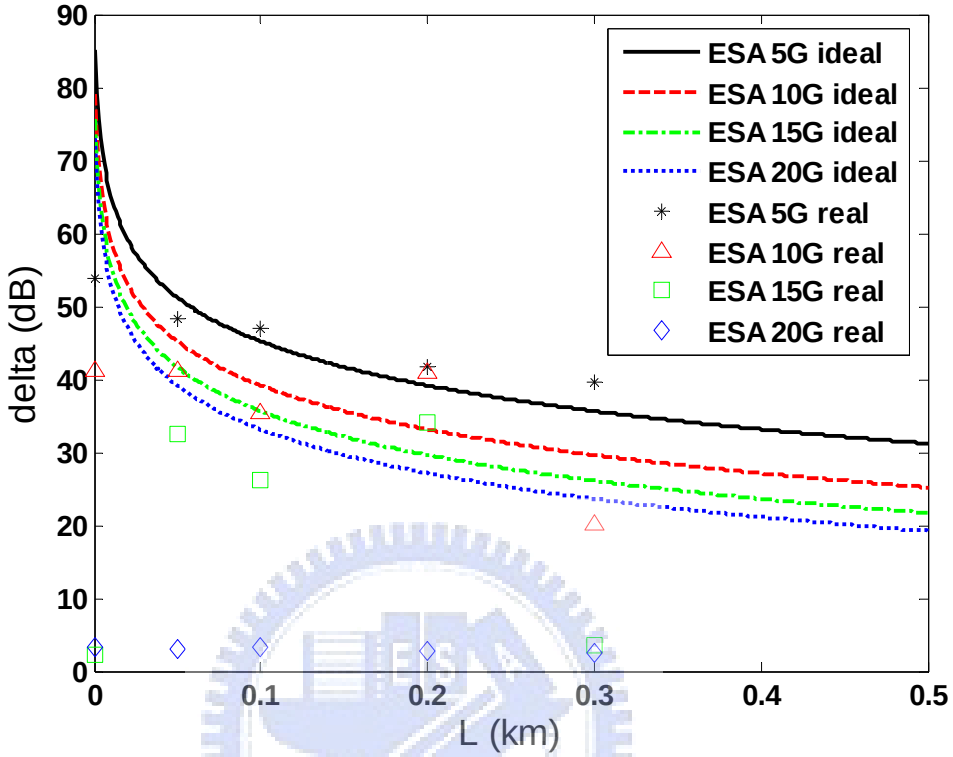

Fig. 3.22 Side-peak ratio △ as a function of the fiber length: experiment (real) and theory (ideal)

From Fig. 3.22 we can understand that ideally the measurement sensitivity is larger for shorter length of test fibers. The reason is because the side-peaks in the RF spectrum don't exist ideally and will be very sensitive to the dispersion-induced changes. In practice, there are still some magnitudes of side-peaks due to the imperfect of the modulators, which will limit the shortest fiber length (or the smallest dispersion) that can be measured.

In high frequencies, the measurement values seem to lose the accuracy because the high frequency terms are smaller and more sensitive to noises. Figure 3.23 shows the electrical signal from the pattern generator and Figure 3.24 shows the optical signal from the pattern generator. The pulse width is 100

(ps) and the edge has some distortion. Such pulse shape distortion may also cause some deviation in high frequency signals, although they may be reduced by filtering.

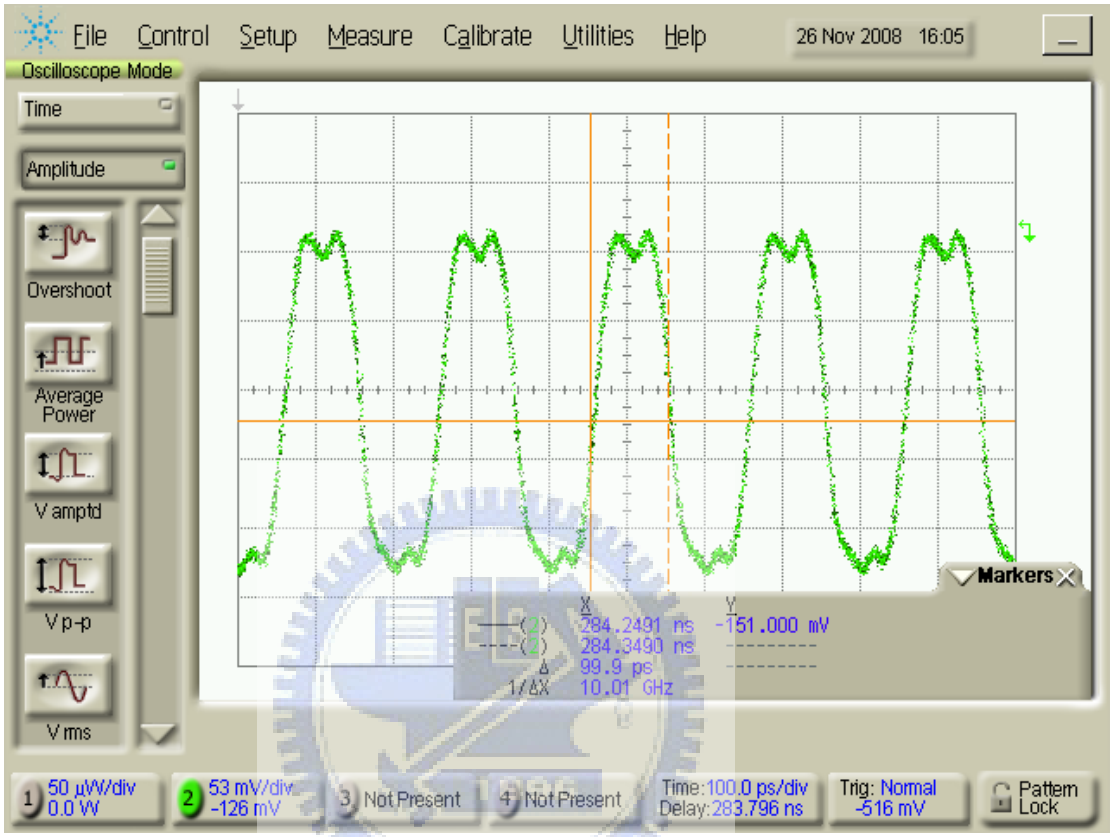

Fig. 3.23 The electrical signal from pattern generator

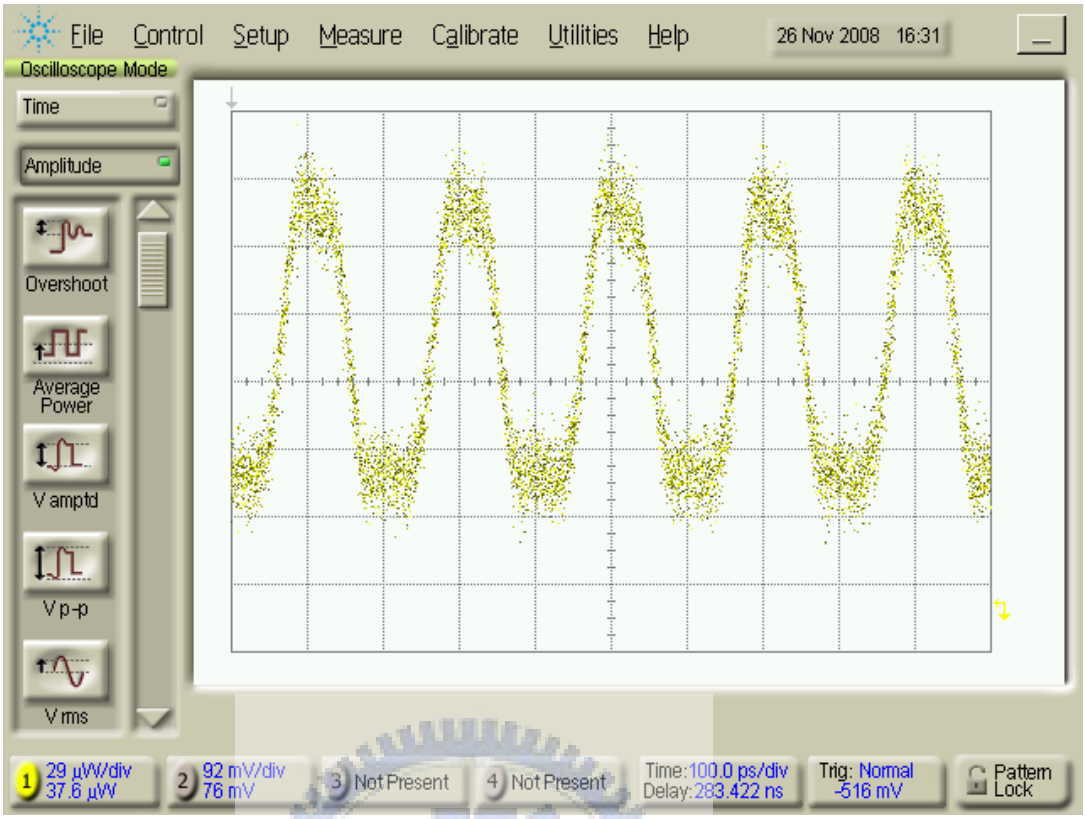

Fig. 3.24 The optical signal from pattern generator

Although we have not succeeded in experimentally demonstrating the GVD measurement by using FSK signals, the feasibility of the measurement method has been verified by simulation. The simulation results are shown in Fig. 3.25.

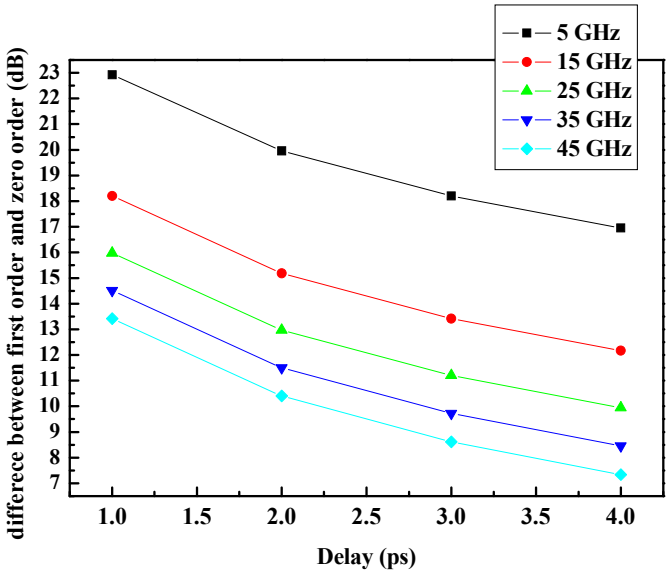

Fig. 3.25 The simulation of GVD measurement

The main simulation parameters are listed in Table 3.3.

Table 3.3 Definition of simulation value

Numerical unit	ps
Wavelength switch frequency	50 MHz
Pulse width	100 ps
Roundtrip time	200 ps
Time window	10^8 ps

If we consider the experimental conditions where the $\Delta\lambda$ is 0.322 nm and the GVD of SMF is 17 ps/km/nm, we can draw the results as in Fig. 3.26.

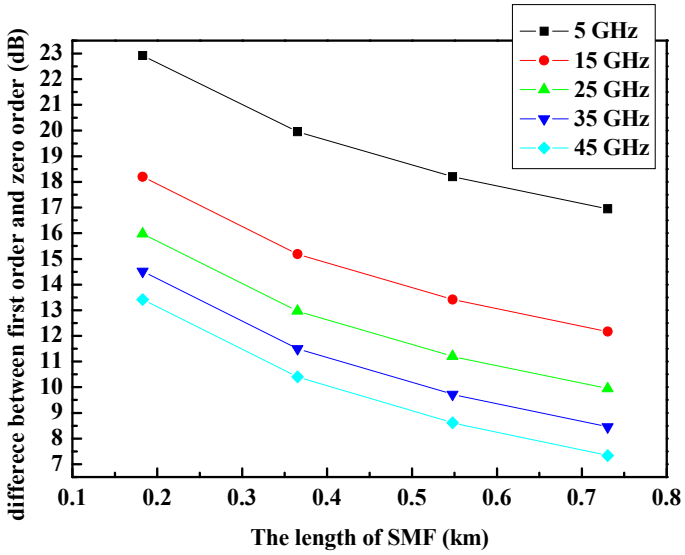

Fig. 3.26 Simulation of GVD measurement as a function of the SMF length

In Fig. 3.26, the tendency of curves is the same as the analytic results in Fig. 3.22.

Reference

[1] C.-T. Lin, Y.-M Lin, J. Chen, S.-P. Dai, P. T. Shih, P.-C. Peng, and S. Chi, "Optical direct-detection OFDM signal generation for radio-over-fiber link using frequency doubling scheme with carrier suppression," Opt. Express, vol 16, pp. 6056-6063, 2008.

Chapter 4

Conclusions

4.1 Summary

In this thesis work, we have proposed and demonstrated a new group velocity measurement method. We use a periodic swept-wavelength pulse light source as the light source for measurement. Theoretically, by using this kind of light source the pulse timing position variation will be increased after the light has passed through a section of dispersive fiber. The pulse timing position variation can then be simply measured by a RF spectrum analyzer. In the experimental side, we have used two kinds of light source to verify the scheme. One is a sinusoidal periodic swept-wavelength modelocked fiber laser source while the other is a periodic bi-wavelength sweeping pulse modulation light source. For the first case, an asynchronous modelocked Er-fiber soliton laser (ASM laser) has been used as the sinusoidal periodic swept-wavelength pulse light source. The detailed derivation and relation formula have been given in Chapter 2. The RF spectrum of the system is of a Bessel form. Successful experimental demonstration has been given in Chapter 3. For the latter case, we use a system consisted of a frequency shifting keying modulator (FSK modulator) and a Mach-Zehnder Modulator (MZM) to be the periodic bi-wavelength sweeping pulse light source. The analytic formula has also been derived in Chapter 2. The RF spectrum of the system is of a sinusoidal form. Successful simulation demonstration has also been given in Chapter 3. One interesting question then is to compare the measurement sensitivity of the two cases so that one can know how to increase the measurement sensitivity when needed. This will be given in the following section.

We can also compare the commercially available modulation phase-shift technique and the periodic wavelength-swept pulse light method developed in the present thesis. The compared characteristics are listed in Table 3.4.

Table 3.4 Comparison between the modulation phase-shift technique and the periodic wavelength-swept pulse light method

Measurement method / specification	MPS (ADVANTEST Q7760)	The new GVD measurement method (ASM Er-fiber laser)
Light source	Tunable laser	Periodic wavelength-swept pulse light source
Observe signal	Phase (RF signal)	Pulse timing position variation (light signal)
Observe instrument	RF network analyzer	RF spectral analyzer
Wavelength measurement resolution (nm)	±0.080	0.835
Wavelength measurement range (nm)	1525 to 1635	1540 ~1560
GVD measurement range unit length	0.1 ps/nm ~ 1 μs/nm	0.875 ps/nm ~ 25.5 ps/nm
Measurement accuracy (ps)	±0.16	±0.125
Measurement accuracy (ps/nm)	×	±0.175
High order dispersion	measurable	immeasurable
Measurement speed	slower	faster
Cost	higher	lower

From the table one can notice some important difference. The MPS can measure the higher order dispersion value owing to the higher wavelength measurement resolution. Thus, the periodic wavelength-swept pulse light method is more suitable to measure the group velocity dispersion (the second

order dispersion) for broadband test components. However, the periodic wavelength-swept pulse light method has better time delay measurement resolution. Also the measurement speed of periodic wavelength-swept pulse light method is faster than MPS because the MPS must scan the RF signal from 40 MHz to 3 GHz per wavelength. Finally, the cost for the MPS method is more expensive then that for the periodic wavelength-swept pulse light method because the MPS method uses a RF network analyzer in the system and the RF network analyzer is more expensive then the RF spectral analyzer.

4.2 Analysis

From Eq. (2.24) and Eq. (2.29) we can get Fig. 4.1 and Fig. 4.2, respectively.

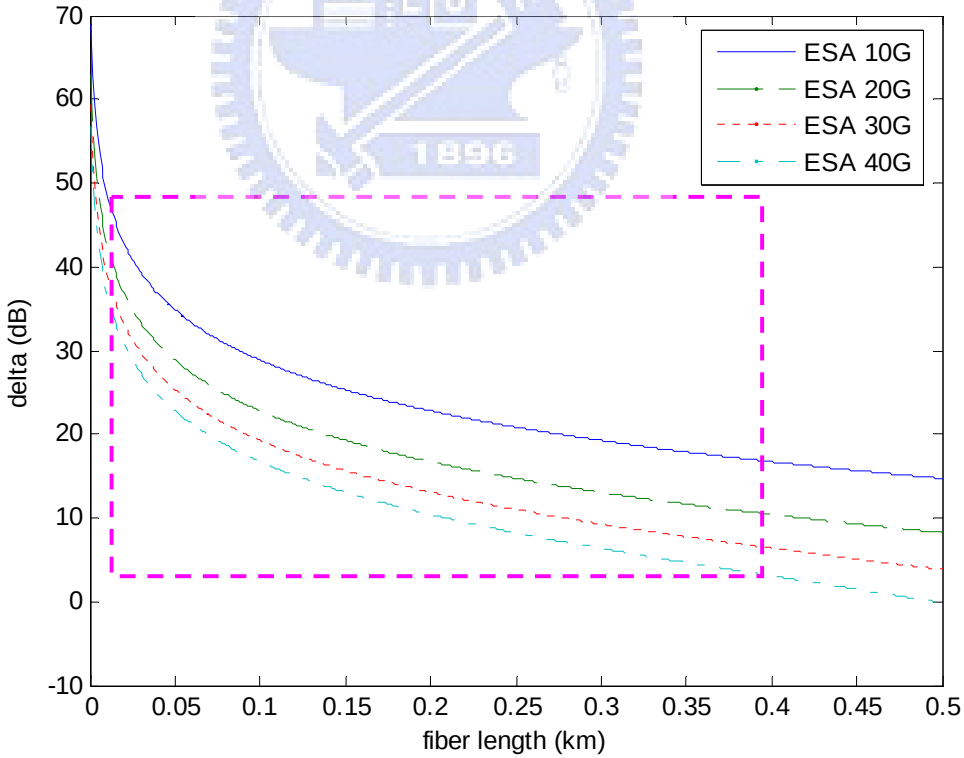

Fig. 4.1 Side-peak ratio in the ideal sinusoidal swept-wavelength pulse light source case

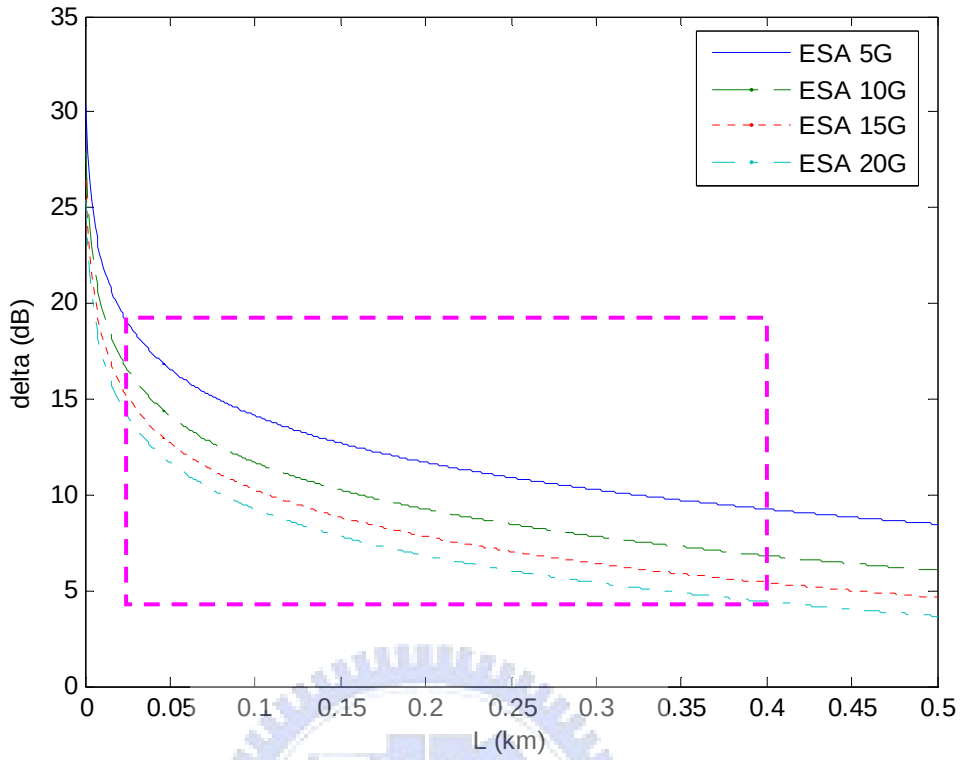

Fig. 4.2 Side-peak ratio in the periodic bi-wavelength sweeping pulse light source case

Comparing Fig. 4.1 and Fig. 4.2, we can know the sensitivity of measurement for shorter fiber lengths is higher in Fig. 4.1 than in Fig. 4.2. But, if we use the ASM laser as the sinusoidal periodic swept-wavelength pulse light source, then the original timing variation δt_0 must be considered. The results are shown in Fig. 4.3 and Fig. 4.4.

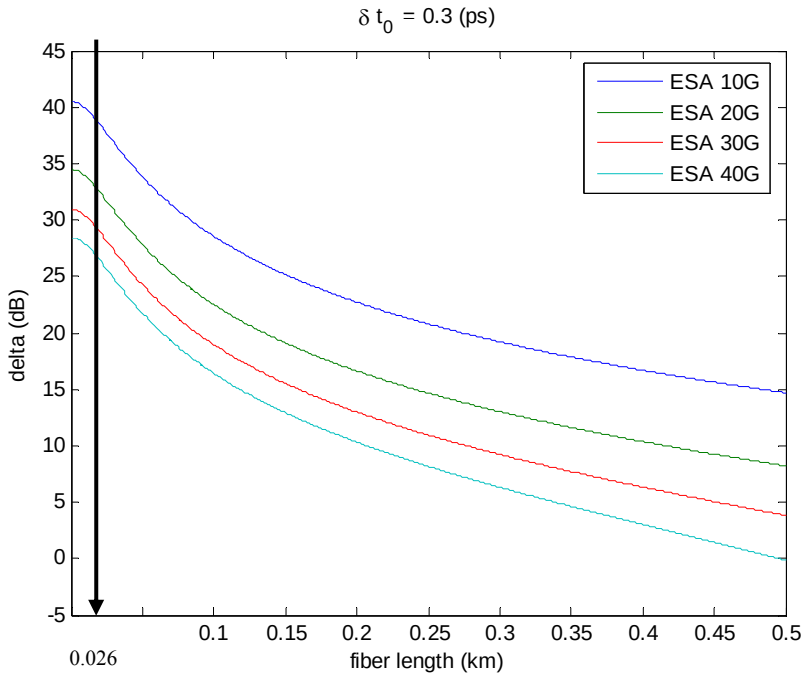

Fig. 4.3 Side-peak ratio in the ASM laser case

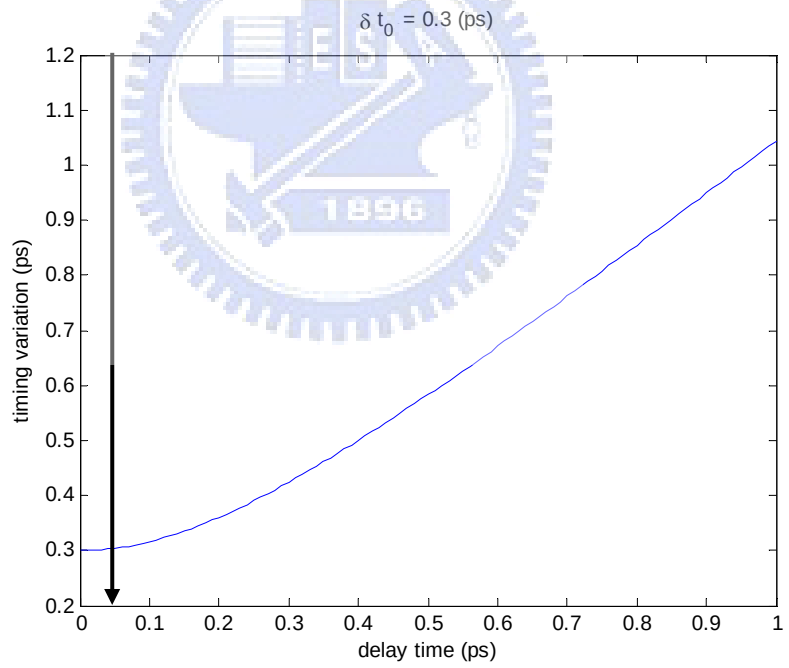

Fig. 4.4 The relation between timing variation and delay time with non-zero δt_0 in the ASM laser case

In Fig. 4.3 and Fig. 4.4, the wavelength variation ($\Delta\lambda$) is equal to 0.677 (nm), the GVD of SMF is 17 ps/km/nm and the original timing variation δt_0 is

0.3 (ps). From Fig. 4.3 and Fig. 4.4, we can see that δt_0 will reduce the measurement sensitivity for short length test fibers. Therefore the original timing variation should be reduced or avoided in the proposed measurement system if possible.

If we use the binary FSK modulation light source to be our measurement source, then in principle the original timing variation from the laser itself can be avoided and thus the measurement sensitivity can be improved. However, the unwanted sidepeaks shown in Fig 3.14 -Fig. 3-17 will limit the achievable measurement sensitivity. These unwanted sidepeaks should be suppressed in the proposed measurement system if possible.

In the FSK experiment, the frequency difference between two double frequency peaks is 0.322 (nm), or equivalently the 20GHz. Fig. 4.5, Fig. 4.6 and Fig. 4.7 show the side-peak ratio relation for different $\Delta\lambda$.

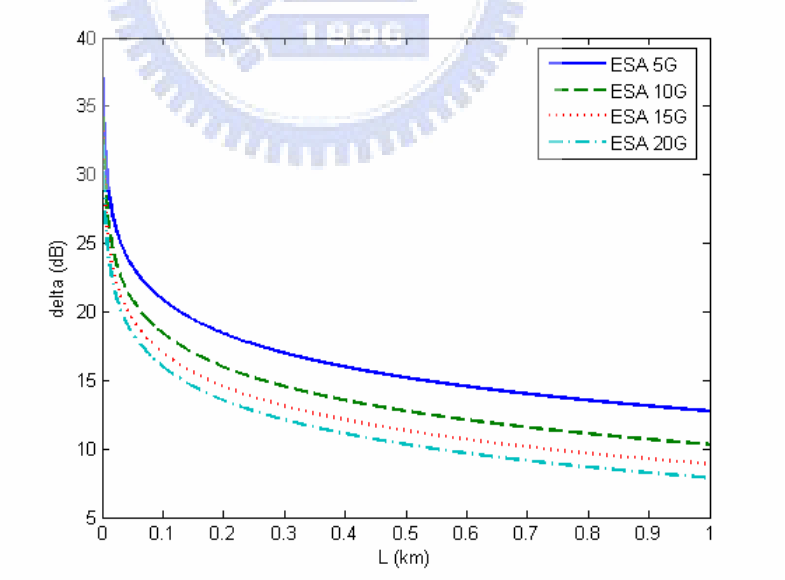

Fig. 4.5 The relation of SMF length and Δ with Δλ=0.1nm

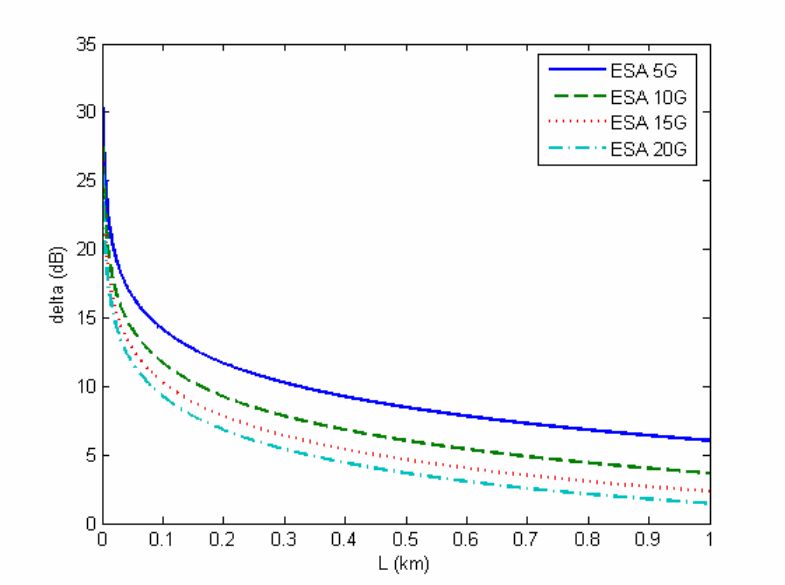

Fig. 4.6 The relation of SMF length and Δ with Δλ=0.677nm

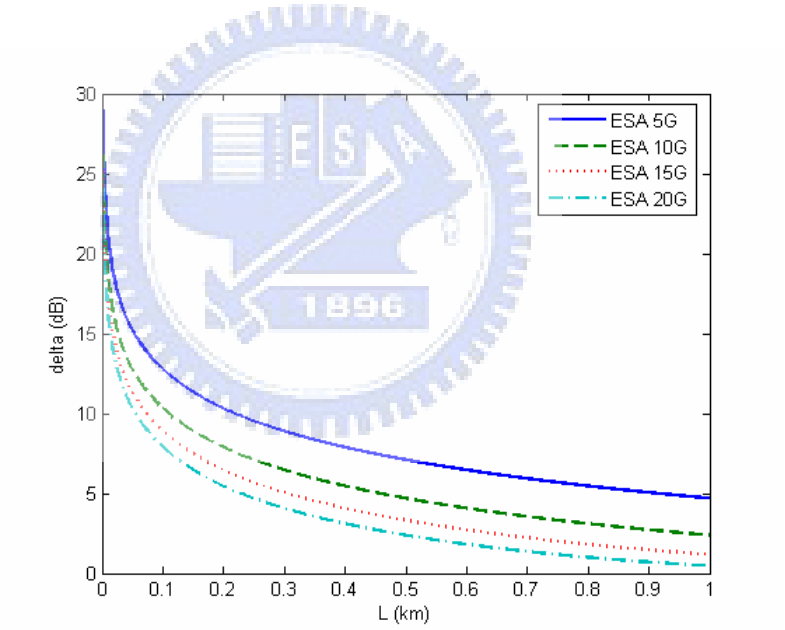

Fig. 4.7 The relation of SMF length and Δ with Δλ=1 nm

From Fig. 4.5, Fig. 4.6 and Fig. 4.7, we can know that the bigger $\Delta\lambda$ will give rise to higher measurement sensitivity. In the ASM fiber laser case, the central frequency variation $\Delta\lambda$ is 0.835 nm, which is achieved by using nonlinear effects and a 10G modulator. In the FSK case, one will need to use a 50GHz modulator for achieving the same $\Delta\lambda$. This shows one important

advantage of the ASM laser for the proposed GVD measurement method.

4.3 Future work

To further exploit the advantages of the ASM laser, we can try to reduce its timing variation δt_0 and to increase its central frequency variation $\Delta\lambda$ as much as possible. In this way the measurement sensitivity of the proposed method can become the biggest advantage when compared to other approaches. Another possible future work is to develop wavelength-swept light sources based on fast wide-range tunable optical filters. In this way the timing variation δt_0 can be reduced and the central frequency difference can also be made very large.